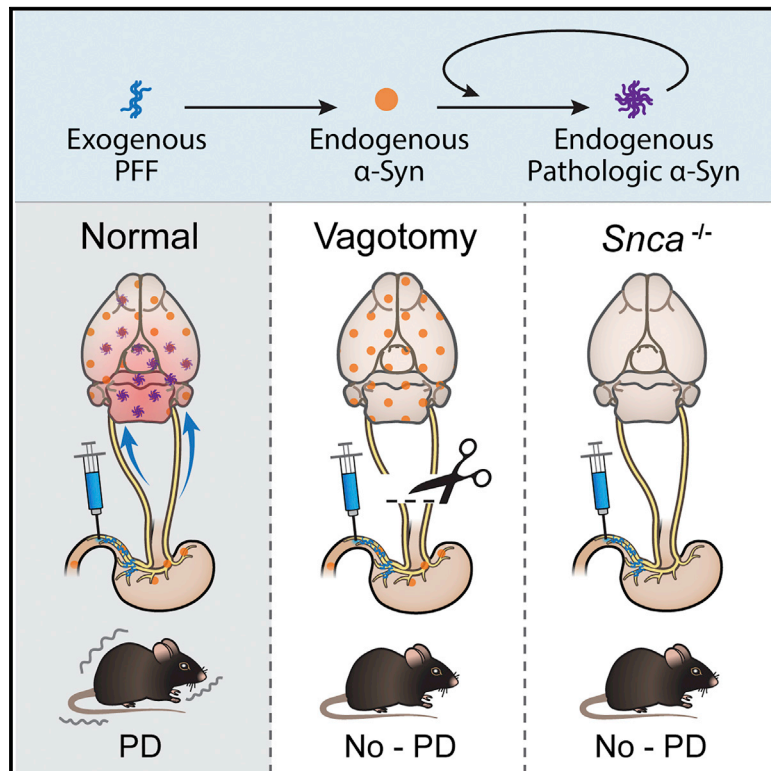


# Transneuronal Propagation of Pathologic $\alpha$ -Synuclein from the Gut to the Brain Models Parkinson's Disease

## Graphical Abstract



## Authors

Sangjune Kim, Seung-Hwan Kwon, Tae-In Kam, ..., Valina L. Dawson, Ted M. Dawson, Han Seok Ko

## Correspondence

tdawson@jhmi.edu (T.M.D.), hko3@jhmi.edu (H.S.K.)

## In Brief

Gut injection of  $\alpha$ -synuclein fibrils converts endogenous  $\alpha$ -synuclein to a pathologic species that spreads to the brain. This leads to features of Parkinson's disease, and vagotomy and  $\alpha$ -synuclein deficiency prevent the neuropathology and neurobehavioral deficits induced by transmitted pathological  $\alpha$ -synuclein.

## Highlights

- Gut-to-brain propagation of pathologic  $\alpha$ -synuclein via the vagus nerve causes PD
- Dopamine neurons degenerate in the pathologic  $\alpha$ -synuclein gut-to-brain model of PD
- Gut injection of pathologic  $\alpha$ -synuclein causes PD-like motor and non-motor symptoms
- PD-like pathology and symptoms require endogenous  $\alpha$ -synuclein

# Transneuronal Propagation of Pathologic $\alpha$ -Synuclein from the Gut to the Brain Models Parkinson's Disease

Sangjune Kim,<sup>1,2,11</sup> Seung-Hwan Kwon,<sup>1,2,11</sup> Tae-In Kam,<sup>1,2</sup> Nikhil Panicker,<sup>1,2</sup> Senthilkumar S. Karuppagounder,<sup>1,2</sup> Saebom Lee,<sup>1,2</sup> Jun Hee Lee,<sup>1,2,9</sup> Wonjoong Richard Kim,<sup>1,2</sup> Minjee Kook,<sup>1,2</sup> Catherine A. Foss,<sup>3</sup> Chentian Shen,<sup>3,10</sup> Hojae Lee,<sup>1,2</sup> Subhash Kulkarni,<sup>4</sup> Pankaj J. Pasricha,<sup>4</sup> Gabsang Lee,<sup>1,2,5</sup> Martin G. Pomper,<sup>3</sup> Valina L. Dawson,<sup>1,2,5,6</sup> Ted M. Dawson,<sup>1,2,5,7,12,\*</sup> and Han Seok Ko<sup>1,2,8,\*</sup>

<sup>1</sup>Neuroregeneration and Stem Cell Programs, Institute for Cell Engineering, Johns Hopkins University School of Medicine, Baltimore, MD 21205, USA

<sup>2</sup>Department of Neurology, Johns Hopkins University School of Medicine, Baltimore, MD 21205, USA

<sup>3</sup>The Russell H. Morgan Department of Radiology and Radiological Science, Johns Hopkins University School of Medicine, Baltimore, MD 21205, USA

<sup>4</sup>Center for Neurogastroenterology, Department of Medicine, The Johns Hopkins University School of Medicine, Baltimore, MD 21205, USA

<sup>5</sup>Solomon H. Snyder Department of Neuroscience, Johns Hopkins University School of Medicine, Baltimore, MD 21205, USA

<sup>6</sup>Department of Physiology, Johns Hopkins University School of Medicine, Baltimore, MD 21205, USA

<sup>7</sup>Department of Pharmacology and Molecular Sciences, Johns Hopkins University School of Medicine, Baltimore, MD 21205, USA

<sup>8</sup>Adrienne Helis Malvin Medical Research Foundation, New Orleans, LA 70130, USA

<sup>9</sup>Present address: Department of Pharmacology and Toxicology, University of Alabama at Birmingham School of Medicine, Birmingham, AL 35294, USA

<sup>10</sup>Present address: Department of Nuclear Medicine, Shanghai Jiao Tong University Affiliated Sixth People's Hospital, Shanghai 200233, China

<sup>11</sup>These authors contributed equally

<sup>12</sup>Lead Contact

\*Correspondence: [tdawson@jhmi.edu](mailto:tdawson@jhmi.edu) (T.M.D.), [hko3@jhmi.edu](mailto:hko3@jhmi.edu) (H.S.K.)

<https://doi.org/10.1016/j.neuron.2019.05.035>

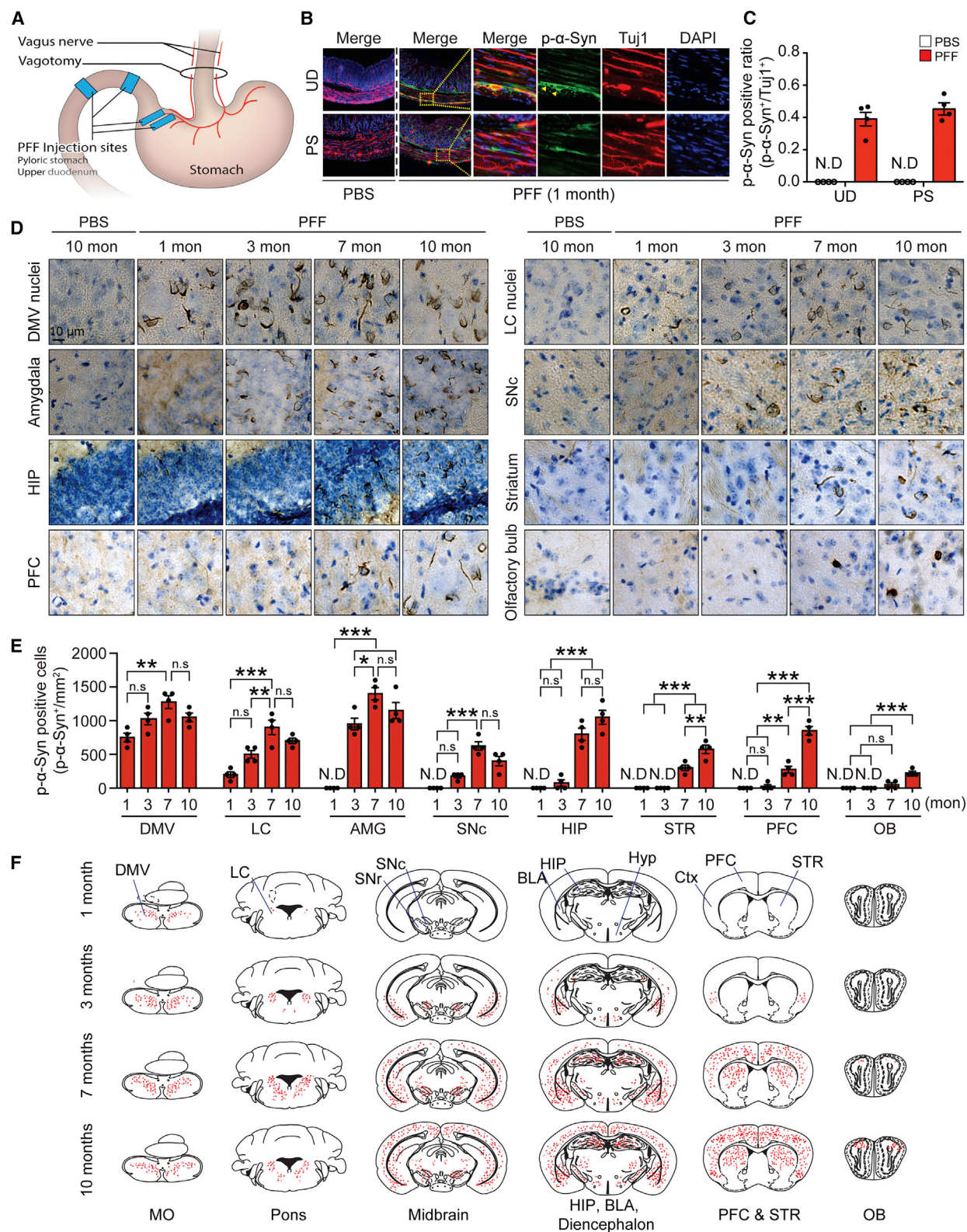
## SUMMARY

Analysis of human pathology led Braak to postulate that  $\alpha$ -synuclein ( $\alpha$ -syn) pathology could spread from the gut to brain via the vagus nerve. Here, we test this postulate by assessing  $\alpha$ -synucleinopathy in the brain in a novel gut-to-brain  $\alpha$ -syn transmission mouse model, where pathological  $\alpha$ -syn preformed fibrils were injected into the duodenal and pyloric muscularis layer. Spread of pathologic  $\alpha$ -syn in brain, as assessed by phosphorylation of serine 129 of  $\alpha$ -syn, was observed first in the dorsal motor nucleus, then in caudal portions of the hindbrain, including the locus coeruleus, and much later in basolateral amygdala, dorsal raphe nucleus, and the substantia nigra pars compacta. Moreover, loss of dopaminergic neurons and motor and non-motor symptoms were observed in a similar temporal manner. Truncal vagotomy and  $\alpha$ -syn deficiency prevented the gut-to-brain spread of  $\alpha$ -synucleinopathy and associated neurodegeneration and behavioral deficits. This study supports the Braak hypothesis in the etiology of idiopathic Parkinson's disease (PD).

## INTRODUCTION

Neurodegenerative diseases characterized by aberrant aggregates of the  $\alpha$ -synuclein ( $\alpha$ -syn) are collectively referred to as synucleinopathies and constitute the second most common form of neurodegenerative dementias (Dodel et al., 2008). Dementia associated with synucleinopathies results from the loss of connectivity within the cognitive circuits, either through cell death or loss of functional connectivity. The work of Braak et al. has further suggested that the neuronal connectivity within this circuit may underlie the path of disease progression and circuit dysfunction associated with Parkinson's disease (PD) (Braak et al., 2003a, 2004) and potentially other synucleinopathies, including dementia with Lewy bodies (DLB).

The Braak hypothesis posits that  $\alpha$ -syn pathology can spread in a stereotyped fashion from the gastrointestinal tract via the vagus nerve to the ventral midbrain, where it selectively kills dopamine (DA) neurons of the substantia nigra pars compacta (SNc). This hypothesized spread of  $\alpha$ -syn pathology is based on the pattern of Lewy body (LB) pathology observed in post-mortem human brain (Braak et al., 2003a). In early stages of PD, LB pathology is most often confined to the olfactory bulb or in the intermediate reticular zone (IZ) and dorsal motor nucleus of the vagus (DMV) in the medulla (Braak et al., 2004). It is only later during disease progression that LB pathology is observed in the midbrain, affecting the SNc and other regions. The progressive spread of LB pathology is consistent with established



(legend on next page)

synaptic connectivity between hindbrain and midbrain neurons (Rogers et al., 1980; Ter Horst et al., 1991) and, based on this pattern, is likely transmitted in a retrograde manner from dendrite to axon. Although the pattern of spread is consistent with retrograde transmission, LB pathology is not observed in all synaptically connected regions (Surmeier et al., 2017).

Growing evidence supports that fibril forms of  $\alpha$ -syn, the principal component of LBs, can be transmitted from cell to cell in a prion-like manner (Lee et al., 2010; Luk et al., 2012; Pan-Montojo et al., 2012; Volpicelli-Daley et al., 2011). Once taken up by a neuron,  $\alpha$ -syn fibrils can act as a template for the aggregation of endogenous  $\alpha$ -syn protein (Karpowicz et al., 2019). The majority of  $\alpha$ -syn in fibrils and in LBs is phosphorylated on serine 129 (pSer129- $\alpha$ -syn) (Anderson et al., 2006; Fujiwara et al., 2002). It is not well established whether all neurons bearing pSer129- $\alpha$ -syn will eventually form LBs or the effect of pSer129- $\alpha$ -syn accumulation has on synaptic efficacy or connectivity.

Recombinant synthesized  $\alpha$ -syn can be aggregated *in vitro* to form fibrils similar in structure to those found *in vivo* (Volpicelli-Daley et al., 2014). These preformed fibrils (PFF) can spread in prion-like manner both in *in vitro* neuronal cultures as well as *in vivo* when injected into the mouse brain, forming pSer129- $\alpha$ -syn-positive LB-like inclusions (Luk et al., 2009, 2012). Injection of PFF into the striatum (STR) of mice results in pSer129- $\alpha$ -syn accumulation and cell death of SNc DA neurons, consistent with retrograde transmission and long-range transport of pathogenic  $\alpha$ -syn (Luk et al., 2012; Mao et al., 2016). Importantly, both the accumulation and spread of pSer129- $\alpha$ -syn requires endogenous  $\alpha$ -syn (Volpicelli-Daley et al., 2011), strongly supporting a prion-like templating mechanism.

Despite the power of PFF injection into the STR or other brain regions of mice as a model to understand the spread of  $\alpha$ -syn-related pathology, current protocols using PFF fail to support the idea that pathologic  $\alpha$ -syn can spread from the gut to brain as described by Braak and colleagues (Braak et al., 2003a, 2004). Although injection into the STR does lead to transport of pathologic  $\alpha$ -syn to SNc DA neurons, there is rarely LB pathology observed in the STR, making this an inaccurate mimic of PD progression (Surmeier et al., 2017). Furthermore, striatal injection of PFF, which leads to SNc pathology, could reflect an anterograde or retrograde process, as both afferent and efferent connectivity exists between the SNc and STR (Calaresi et al., 2014; Watabe-Uchida et al., 2012). Recently, a study

was performed where PFF injections were made into the olfactory bulb, one of Braak's posited sites of PD's initiation, and although the appearance of pSer129- $\alpha$ -syn pathology was extensive, there was no accumulation in the SNc (Rey et al., 2016). To address the need for a model that recapitulates the features of PD and captures the spread of pathologic  $\alpha$ -syn as monitored by pSer129- $\alpha$ -syn, we developed a method where PFF are injected into the muscularis layer of the pylorus and duodenum, mimicking the spread of pathologic  $\alpha$ -syn observed in PD (Gelpi et al., 2014; Klingelhoefer and Reichmann, 2015). The pathologic  $\alpha$ -syn pathology as assessed by pSer129- $\alpha$ -syn immunoreactivity spreads as Braak proposed, being observed first in the DMV. Later pSer129- $\alpha$ -syn is observed in caudal portions of the hindbrain, including the locus coeruleus (LC), and later to the basolateral amygdala (BLA), dorsal raphe nucleus (DRN), and SNc. Truncal vagotomy (TV) prevents the spread of pathologic  $\alpha$ -syn to the brain. In addition, no transmission is observed in  $\alpha$ -syn knockout (*Snc $\alpha$ <sup>-/-</sup>*) mice. These observations are consistent with the seeding and misfolding of endogenous  $\alpha$ -syn, leading to retrograde, polysynaptic spreading of pathologic  $\alpha$ -syn from the gut via the vagus nerve to the SNc and beyond, mimicking with some accuracy what is seen in clinical synucleinopathies, like PD and DLB.

## RESULTS

### Spread of Pathologic $\alpha$ -syn from the Gut to the Brain

Evidence from human postmortem studies suggests that  $\alpha$ -syn pathology could spread from the enteric nervous system (ENS) and propagate to the CNS through the vagal nerve (Braak et al., 2003b). To test this postulate experimentally, mouse  $\alpha$ -syn PFF were injected into the muscle layers of the pylorus and duodenum, which are densely innervated by the vagus nerve (Berthoud et al., 1991). Prior to injection of PFF, trypan blue was injected between the longitudinal and intermediate muscle layers of the pylorus and duodenum to determine the volume that could be injected without substantial damage or leakage (Figure S1A). Based on these experiments, it was determined that 3  $\mu$ L could be safely injected. As such, 2.5  $\mu$ L of PFF (2.5  $\mu$ g/ $\mu$ L) was injected in two different locations in the pylorus and two different locations in the duodenum between the longitudinal and intermediate muscle layers where the myenteric plexus resides (Figure 1A; Furness, 2012). The average size of

**Figure 1.  $\alpha$ -syn PFF Injection into the Gut Triggers Progressive Spreading of  $\alpha$ -syn Pathology to the Enteric Nervous System followed by Spread to Connected Brain Regions**

(A) Overview of the site of injection and vagotomy.

(B) Representative double-immunostaining for pSer129- $\alpha$ -syn (green) and Tuj-1 (red) in the upper duodenum (UD) and pyloric stomach (PS) after 1 month post-injection.

(C) Quantification of pSer129- $\alpha$ -syn-positive neurons normalized to Tuj-1-positive neurons in the upper duodenum and pyloric stomach ( $n = 4$ ).

(D) Brain distribution of pSer129- $\alpha$ -syn accumulation in mice that received  $\alpha$ -syn PFF in the gut. pSer129- $\alpha$ -syn immunohistochemistry from the dorsal motor nucleus of the vagus to the olfactory bulb of  $\alpha$ -syn PFF gastrointestinal-injected mice sacrificed at 1, 3, 7, and 10 months post-injection.

(E) Quantification of pSer129- $\alpha$ -syn immunoreactivity shown in (D) ( $n = 4$ ).

(F) Diagram illustrating the CNS distribution of pSer129- $\alpha$ -syn representing  $\alpha$ -syn pathology (red dots) in the brain from coronal sections from 1, 3, 7, and 10 months post-injection.

Error bars represent the mean  $\pm$  SEM. Statistical significance was determined using a two-way ANOVA followed by post hoc Bonferroni test for multiple group comparison. \*\*\* $p < 0.001$ . BLA, basolateral amygdala; CPu, upper caudate-putamen; Ctx, cortex; DG, dentate gyrus; DMV, dorsal motor nucleus of the vagus; HIP, hippocampus; LC, locus coeruleus; MO, medulla oblongata; N.D., not detected; OB, olfactory bulb; PFC, prefrontal cortex; PS, pyloric stomach; SNc, substantia nigra pars compacta; SNr, substantia nigra pars reticulata; STR, striatum; UD, upper duodenum. See also Figures S1–S3.

PFF as determined by transmission electron microscopy was  $64.7 \pm 1.7$  nm (Figures S1B and S1C). The myenteric plexus of the pylorus and duodenum were examined and demonstrate pSer129- $\alpha$ -syn immunostaining in myenteric neurons, indicating that the PFF are templating the endogenous  $\alpha$ -syn to misfold (Figures 1B and 1C). pSer129- $\alpha$ -syn immunostaining was used to monitor the progression of pathologic  $\alpha$ -syn from the gut to the brain. 1 month after PFF injection, pSer129- $\alpha$ -syn immunostaining is observed in the DMV of the medulla oblongata (MO) and the LC of the pons (Figures 1D–1F and S1D). Immunoblot analysis confirms that pSer129- $\alpha$ -syn is observed in the MO, pyloric stomach (PS), and upper duodenum (UD) (Figures S2A–S2D). Within 3 months, pSer129- $\alpha$ -syn continues to accumulate in the DMV of the MO and the LC of the pons (Figures 1D–1F and S1D) and via immunoblot in the MO and pons (Figures S2E–S2G) and is now observed in the amygdala (Figures 1D–1F, S1D, S2G, and S2H) and is starting to accumulate in the SNc of the ventral midbrain (VMB) (Figures 1D–1F, S1D, S2G, and S2I). Small accumulations of pSer129- $\alpha$ -syn immunostaining are observed in the hypothalamus and prefrontal cortex (PFC) (Figures 1D–1F, S1D, S2G, and S2J). 7 months after PFF injection, an extensive amount of pSer129- $\alpha$ -syn is observed in all regions mentioned and in addition the hippocampus (HIP) and STR (Figures 1D–1F, S1D, and S2E–S2L). At 7 months, pSer129- $\alpha$ -syn is beginning to be observed in the olfactory bulb (OB) (Figures 1D–1F, S1D, S2G, and S2M). 10 months after PFF injection, pSer129- $\alpha$ -syn continues to increase in the HIP, PFC, OB, and STR and is decreased in the amygdala, VMB, and MO (Figures 1D–1F, S1D, and S2E–S2M). In addition, there is a reverse correlation between the levels of soluble  $\alpha$ -syn and the levels of insoluble  $\alpha$ -syn, which show a similar pattern of temporal distribution to pSer129- $\alpha$ -syn (Figures S2A–S2O). We compared the ability of mouse monomeric  $\alpha$ -syn, mouse  $\alpha$ -syn PFF versus human  $\alpha$ -syn PFF to cause pSer129- $\alpha$ -syn in tyrosine hydroxylase (TH)-positive neurons of the VMB 3 months after injections into the PS and UD. We find that mouse  $\alpha$ -syn PFF-injected mice show pathological  $\alpha$ -syn accumulation in the SNc 3 months post-injection and mouse  $\alpha$ -syn monomer and human  $\alpha$ -syn PFF-injected mice fail to elicit pathological  $\alpha$ -syn accumulation in the VMB at the same time point (Figures S3A–S3D).

### Loss of DA Neurons Following PFF Injection into the Gut

The integrity of the dopaminergic system was monitored following PFF injection into the PS and UD. TH- and Nissl-positive cell counts were monitored by unbiased stereologic methods, and at 1 and 3 months after PFF injections, there is no significant loss of the number of TH- or Nissl-positive cells (Figures 2A–2C). In contrast, at 7 months, there is a significant loss of DA neurons in the SNc as indicated by a reduction of TH- and Nissl-positive cell counts. The loss of DA neurons progresses as there is a further reduction of TH and Nissl cell counts at 10 months following PFF injections (Figures 2A–2C). Accompanying the loss of DA neurons is a reduction of TH immunoreactivity in the STR (Figures S3E and S3F). There is also a reduction of TH and DA transporter (DAT) as determined by immunoblot in the VMB (Figures 2D and 2E) and STR (Figures S3G and S3H). High-performance liquid chromatography (HPLC) indicates that striatal DA is significantly reduced at 3 months and is further reduced

at 7 months (Figure 2F). The DA metabolite, DOPAC, is significantly reduced at 3 and 7 months (Figure S3I). At 7 months, the DA metabolites, homovanillic acid (HVA) (Figure S3J) and 3-methoxytyramine (3MT; Figure S3K), are significantly reduced. ( $^{123}$ I) ioflupane (iodine-123-fluoropropyl [FP]-carbomethoxy-3  $\beta$ -[4-iodophenyl]tropane) imaging via single photon emission computed tomography (SPECT)/computed tomography (CT) confirms the reduction in striatal DAT induced by PFF injections into the PS and UD (Figures 2G and 2H).

### The Vagus Nerve and Endogenous $\alpha$ -syn Are Required for the Gut-to-Brain Transmission of Pathologic $\alpha$ -syn

To evaluate whether pathologic  $\alpha$ -syn is transported via the vagus nerve and whether endogenous  $\alpha$ -syn is required for the spread of pathologic  $\alpha$ -syn into higher brain structures, experiments were conducted following truncal vagotomy after PFF injection in wild-type (WT) mice or PFF injection in *Snca*<sup>−/−</sup> mice. After PFF or PBS injection into WT mice, a truncal vagotomy (TV) was performed by cutting the left and right vagal nerve fibers immediately proximal to the UD and in the neck. To confirm a successful TV, the number of choline acetyltransferase (ChAT)-positive cholinergic neurons in the DMV in PFF- or PBS-injected WT mice after TV were assessed. 7 months after TV, there is a 65% reduction in the number of ChAT-positive cell bodies in the DMV in both PFF- and PBS-injected mice compared to WT mice with an intact vagal nerve (non-TV; Figures S4A and S4B). 3 months after TV, there is no induction of the gastrointestinal hormone, ghrelin, after 48 h of food deprivation (Figure S4C), consistent with prior reports (Williams et al., 2003). Interestingly, there is a reduction in serum ghrelin levels in PFF-injected WT mice with an intact vagus nerve, which is consistent with the observation in PD patients (Song et al., 2017). Food intake and body weight are also reduced in PFF-injected mice as well as TV mice (Figures S4D and S4E). There is also a reduction in the total fecal pellet output and moisture content of the fecal matter in PFF-injected non-TV and TV mice (Figures S4F–S4H). Taken together, these results suggest that the vagotomy was successfully performed.

To assess  $\alpha$ -syn pathology, PFF- or PBS-injected mice that were subjected to TV were examined 7 months later and compared to PFF- or PBS-injected WT or *Snca*<sup>−/−</sup> mice. 7 months after PFF injection, pSer129- $\alpha$ -syn is significantly increased in the UD in WT and TV mice but is not detected in the *Snca*<sup>−/−</sup> mice, similar to PBS-injected controls as determined by immunoblot analyses (Figures S5A and S5B). In the SNc, 7 months after PFF injection, pSer129- $\alpha$ -syn is detected in WT mice, but not TV mice or *Snca*<sup>−/−</sup> mice (Figures 3A and S5C). The integrity of the dopaminergic system was monitored by unbiased stereologic counts of TH- and Nissl-positive neurons in the SNc. PFF injection causes a significant loss of DA neurons, which is completely prevented by TV or the absence of *Snca* (Figures 3B–3D). PFF injection into WT mice also causes a significant loss of TH and DAT protein levels in the VMB, although there is no loss in TV or *Snca*<sup>−/−</sup> mice (Figures S5D and S5E). HPLC analysis demonstrates a loss of DA (Figure 3E) and DA metabolites HVA (Figure S5F), 3MT (Figure S5G), and DOPAC (Figure S5H) in the STR of PFF-injected WT mice, but not PFF-injected TV or *Snca*<sup>−/−</sup> mice. Accompanying the loss

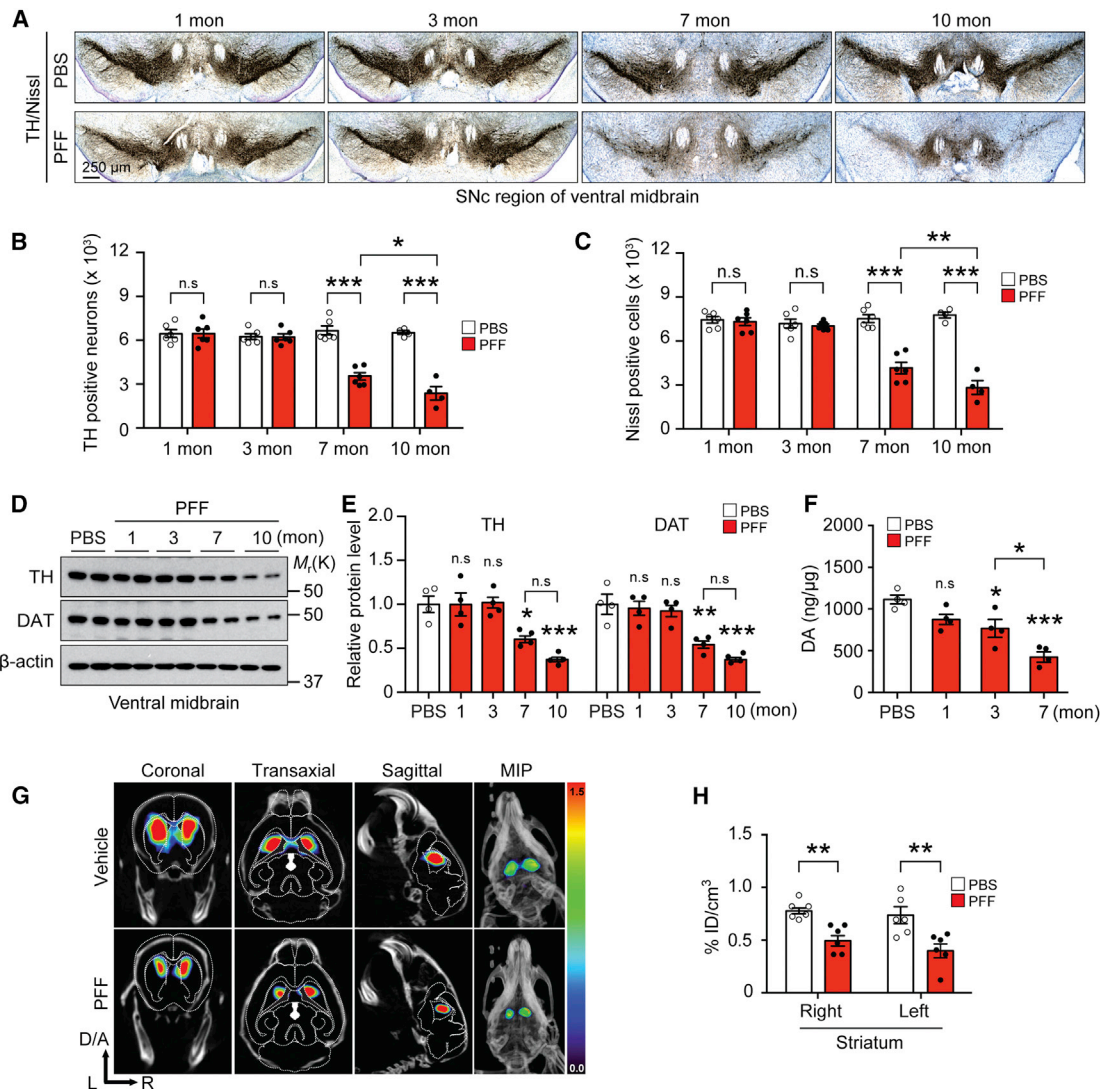


**Figure 2.  $\alpha$ -syn PFF Injection into the Gut Leads to Progressive PD-like Pathology**

(A) Representative photomicrographs from coronal mesencephalon sections containing TH-positive neurons in the SNc region of 1, 3, 7, and 10 months after gastrointestinal injection of  $\alpha$ -syn PFF.

(B and C) Stereology counts of (B) TH- and (C) Nissl-positive neurons in the SNc region of one hemisphere. Unbiased stereological counting was performed in the SNc region ( $n = 4-6$ ).

(D) Representative immunoblots of TH, DAT, and  $\beta$ -actin in the ventral midbrain over time.

(E) Quantification of TH and DAT protein levels normalized to  $\beta$ -actin ( $n = 4$ ).

(F) DA concentrations in the STR of PBS and  $\alpha$ -syn PFF gastrointestinal-injected mice over time as measured by HPLC ( $n = 4$ ).

(G) DAT SPECT/CT scans showing representative images after PBS and  $\alpha$ -syn PFF gastrointestinal-injected mice at 7 months.

(H) Quantification of DAT SPECT/CT results ( $n = 6$ ).

Error bars represent the mean  $\pm$  SEM. Statistical significance was determined using a two-way ANOVA followed by post hoc Bonferroni test for multiple group comparison. \* $p < 0.05$ ; \*\* $p < 0.01$ ; \*\*\* $p < 0.001$ . n.s., not significant. See also Figure S3.

of DA and DA metabolites is a significant loss of TH immunoreactivity (Figures S5I and S5J) and TH and DAT protein levels (Figures S5K and S5L) in the STR of PFF-injected WT mice, but not PFF-injected TV or *Snca*<sup>-/-</sup> mice (Figures S5I–S5L). Behavioral analysis indicates that PFF-injected WT mice have a significantly decreased latency to fall by the rotarod test (Figure 3F), a significantly increased time on the pole test (Figure 3G; Video S1), significantly decreased forelimb strength (Figure 3H), and signif-

icantly decreased forelimb and hindlimb grip strength (Figure S5M), and PFF-injected TV or *Snca*<sup>-/-</sup> mice have no deficits (Figures 3F–3H and S5M).

### Transmission of Pathologic $\alpha$ -syn from the Gut to the Brain Leads to Cognitive Deficits

In addition to the well-known motor deficits in PD, key features of PD also include non-motor symptoms involving cognitive

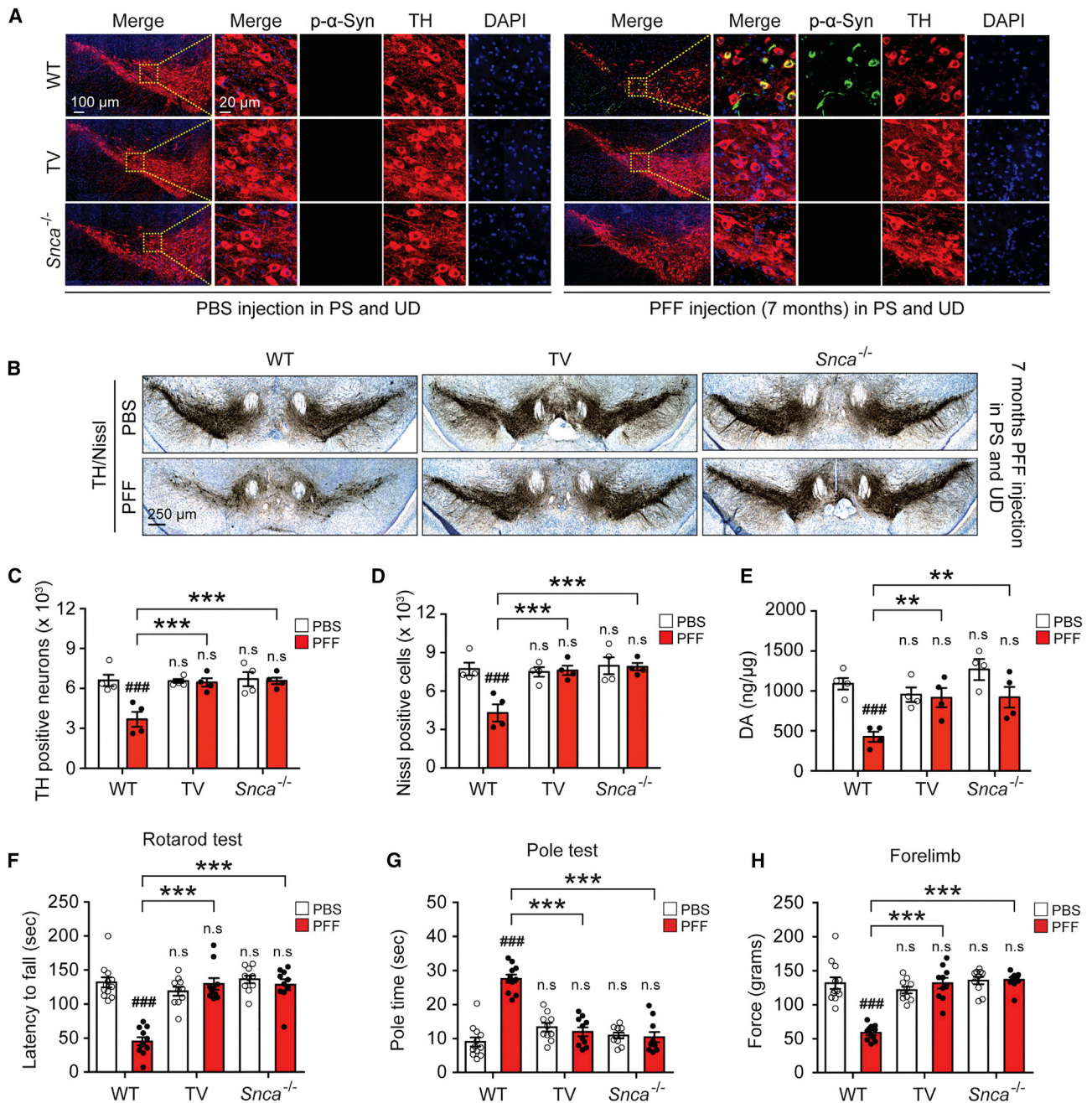


**Figure 3. Vagotomy and  $\alpha$ -syn Deficiency Prevents PD-like Pathology Induced by  $\alpha$ -syn PFF Injection into the Gut**

(A) Representative double immunostaining for pSer129- $\alpha$ -syn (green) and TH (red) in SNc.

(B) Representative photomicrographs from coronal mesencephalon sections containing TH-positive neurons in the SNc region of 7 months after  $\alpha$ -syn PFF gastrointestinal-injected WT, vagotomy (TV), and *Snca*<sup>-/-</sup> mice.

(C and D) Stereology counts of (C) TH- and (D) Nissl-positive neurons in the SNc region of one hemisphere. Unbiased stereological counting was performed in the SNc region of WT, TV, and *Snca*<sup>-/-</sup> mice (n = 4).

(E) DA concentrations in the STR of PBS and  $\alpha$ -syn PFF gastrointestinal-injected WT, vagotomy, and *Snca*<sup>-/-</sup> mice as determined by HPLC (n = 4).

(F–H) Behavioral assessment at 7 months after PBS and  $\alpha$ -syn PFF gastrointestinal-injected WT (n = 11–12), TV (n = 10), and *Snca*<sup>-/-</sup> mice (n = 10). Results of mice on the (F) rotarod test, (G) pole test, and (H) forelimb grip strength test are shown.

Error bars represent the mean  $\pm$  SEM. Statistical significance was determined using a two-way ANOVA followed by post hoc Bonferroni test for multiple group comparison. ###p < 0.001 versus PBS gastrointestinal-injected WT group. \*\*p < 0.01; \*\*\*p < 0.001 versus  $\alpha$ -syn PFF gastrointestinal-injected WT mice group. n.s., not significant. See also [Figures S4 and S5](#) and [Video S1](#).

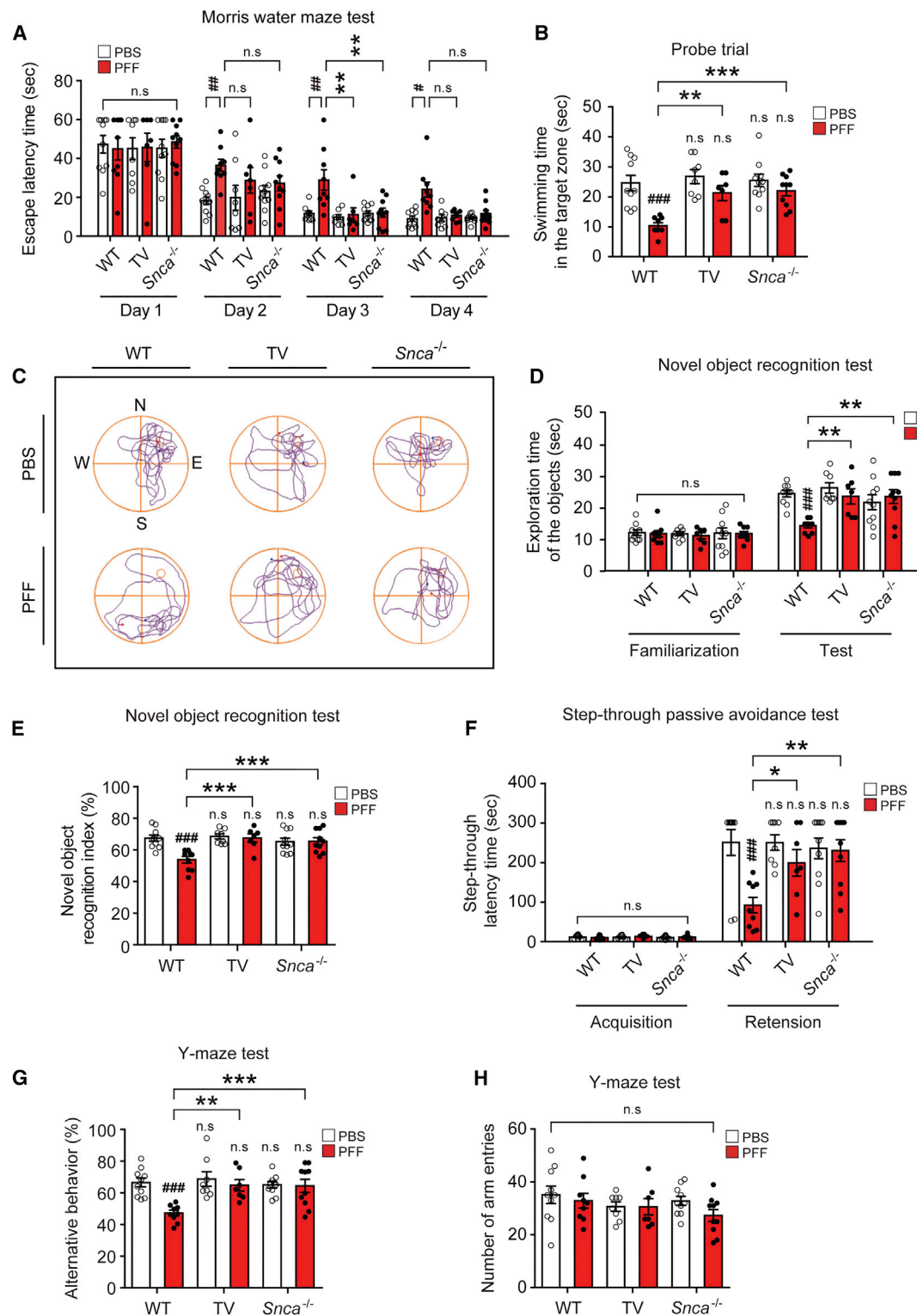


**Figure 4. Vagotomy and  $\alpha$ -syn Deficiency Prevents Cognitive Deficits Induced by  $\alpha$ -syn PFF Injection into the Gut**

Cognitive behavioral assessments 7 months after PBS and  $\alpha$ -syn PFF gastrointestinal injection in WT (n = 9–10), vagotomy (TV; n = 7–8), and *Snca*<sup>-/-</sup> mice (n = 10).

(legend continued on next page)

and behavioral deficits (Pfeiffer, 2003; Ponsen et al., 2004; Reissler and Mayberg, 2007). We assessed spatial learning and memory by the Morris water maze task 7 months after PFF or PBS injection (Figure 4A). On days 3 and 4 of exposure to the Morris water maze, the PFF-injected WT mice have a significantly increased escaped latency time compared to the PBS-treated WT mice (Figure 4A). Both the PFF-injected TV and *Snca*<sup>-/-</sup> mice have escape latency times comparable to PBS-injected WT mice (Figure 4A). Following the last day of trial sessions (day 5), both PFF-injected TV and PFF-injected *Snca*<sup>-/-</sup> mice have significantly increased swimming time and paths in the target quadrant after the platform was removed, similar to PBS-injected WT mice compared to PFF-injected WT mice (Figures 4B and 4C; Video S2). There are no significant differences in the swimming speed and total distance traveled between all experimental groups (Figures S6A and S6B). Next, a novel object recognition test was conducted to assess recognition memory (Bevins and Besheer, 2006). PFF injection significantly decreases the exploration time and recognition index for novel objects in WT mice, and PFF-injected TV or *Snca*<sup>-/-</sup> mice have no deficits, similar to PBS-injected WT mice (Figures 4D and 4E). The familiarization trial of exploration of the objects do not significantly differ between the experimental groups (Figure 4D). To assess hippocampal-dependent contextual or amygdala-dependent fear conditioning, the step-through latency time was assessed using the passive avoidance test (Arias et al., 2015; Eagle et al., 2016). The PFF-treated WT mice have a lower step-through latency time than the PBS-treated WT mice (Figure 4F). Both PFF-injected TV and *Snca*<sup>-/-</sup> mice are similar to PBS-injected mice in this task (Figure 4F). Short-term or working memory was investigated with the spontaneous alternating behavior by the Y-maze test. The percentage of alternating behavior in the PFF-injected WT mice is significantly lower than that of the PBS-injected WT mice. There are no deficits in the PFF-injected TV or *Snca*<sup>-/-</sup> mice (Figures 4G and 4H). Pathologic  $\alpha$ -syn, as assessed by pSer129- $\alpha$ -syn immunoblot (Figures S2G and S2K) and immunostaining (Figures S6C and S6D) is elevated in the hippocampus 7 months post-injection of PFF into the PS and UD. Accompanying the elevation of hippocampal pSer129- $\alpha$ -syn immunostaining is a reduction in NeuN immunostaining (Figures S6C and S6E). PFF-injected TV or *Snca*<sup>-/-</sup> mice fail to exhibit increased pSer129- $\alpha$ -syn immunostaining or a reduction in NeuN immunostaining (Figures S6C–S6E).

### Transmission of Pathologic $\alpha$ -syn from the Gut to the Brain Leads to Deficits in Psychological Behavior

Mice were subjected to the nest-building test, which assesses fine motor dexterity, cognition, and emotional state while imposing minimal stress on the animal (Fleming et al., 2004; Wu et al., 2016). The PFF-injected WT mice show a significant decrease in the nest building score and increased unused nestlet material compared to the PBS-injected WT mice (Figures 5A–5C). PFF-injected TV or *Snca*<sup>-/-</sup> mice perform in a similar manner to the PBS-injected WT mice (Figures 5A–5C). Anxiety was measured by the elevated plus maze and open field tests (Pellow and File, 1986; Sakata et al., 2010). On the elevated plus maze, the percentage of arm entries and time spent in the open arm are significantly decreased in the PFF-injected WT mice when compared to the PBS-injected WT mice (Figures 5D–5F; Video S3). Both PFF-injected TV and *Snca*<sup>-/-</sup> mice perform in a manner similar to PBS-injected WT mice (Figures 5D–5F). The open field test was performed to evaluate locomotor and anxiety-like behaviors. The percentage of time spent, entries, and travel paths in the center zone are significantly decreased in the PFF-injected WT mice compared to the PBS-injected WT mice (Figures 5G–5I, S6F, and S6G; Video S4). Both PFF-injected TV and *Snca*<sup>-/-</sup> mice perform in a manner similar to PBS-injected WT mice (Figures 5G–5I, S6F, and S6G). To assess depressive-like symptoms, the mice were evaluated by the tail suspension test and forced swim test (Figures 5J and 5K; Video S5; Cryan et al., 2005; Porsolt et al., 1978; Steru et al., 1985). The PFF-injected WT mice show increased immobility times in the tail suspension test and forced swim test compared to PBS-injected WT mice (Figures 5J and 5K). Both PFF-injected TV and *Snca*<sup>-/-</sup> mice perform in a manner similar to PBS-injected WT mice (Figures 5J and 5K). To evaluate olfactory dysfunction, the mice were evaluated 9 months after PFF or PBS injection using the buried pellet task after a period of food deprivation (Fleming et al., 2008; Talaga et al., 2017). 3 to 4 days after food deprivation, the PBS-injected WT mice more rapidly find the buried pellet when compared to the PFF-injected WT mice (Figures 6A–6C). Both PFF-injected TV and *Snca*<sup>-/-</sup> mice perform in a manner similar to PBS-injected WT mice (Figures 6A–6C).

### DISCUSSION

The major findings of this study provide support for the concept that pathologic  $\alpha$ -syn is capable of spreading from the

(A and B) Escape latency time (A) and probe trial session (B) in the Morris water maze test.

(C) Representative swimming paths of mice from each group in the Morris water maze test (MWM) on the probe trial day 5. The mice were then given two trial sessions each day for 4 consecutive days, with an inter-trial interval of 15 min, and the escape latencies were recorded. This parameter was averaged for each session of trials and for each mouse.

(D and E) Exploration time of the objects (D) and percentage of novel object recognition index (E) in the novel object recognition test.

(F) Effect of TV and  $\alpha$ -syn deficiency on  $\alpha$ -syn PFF-induced hippocampal-dependent contextual or amygdala-dependent fear conditioning learning and memory in the step-through passive avoidance test. The time taken for a mouse to enter the dark compartment after door opening was defined as latency for both training and test trials.

(G and H) Effect of TV and  $\alpha$ -syn deficiency on  $\alpha$ -syn PFF-induced short-term or working memory in the Y-maze test. Percentage of alternative behavior (G) and number of arm entries (H) in the Y-maze test.

Error bars represent the mean  $\pm$  SEM. All behavior tests were analyzed by two-way ANOVA followed by post hoc Bonferroni test for multiple group comparison. # $p < 0.05$ ; ## $p < 0.01$ ; ### $p < 0.001$  versus PBS gastrointestinal-injected WT group. \* $p < 0.05$ ; \*\* $p < 0.01$ ; \*\*\* $p < 0.001$  versus  $\alpha$ -syn PFF gastrointestinal-injected WT group n.s., not significant. See also Figure S6 and Video S2.

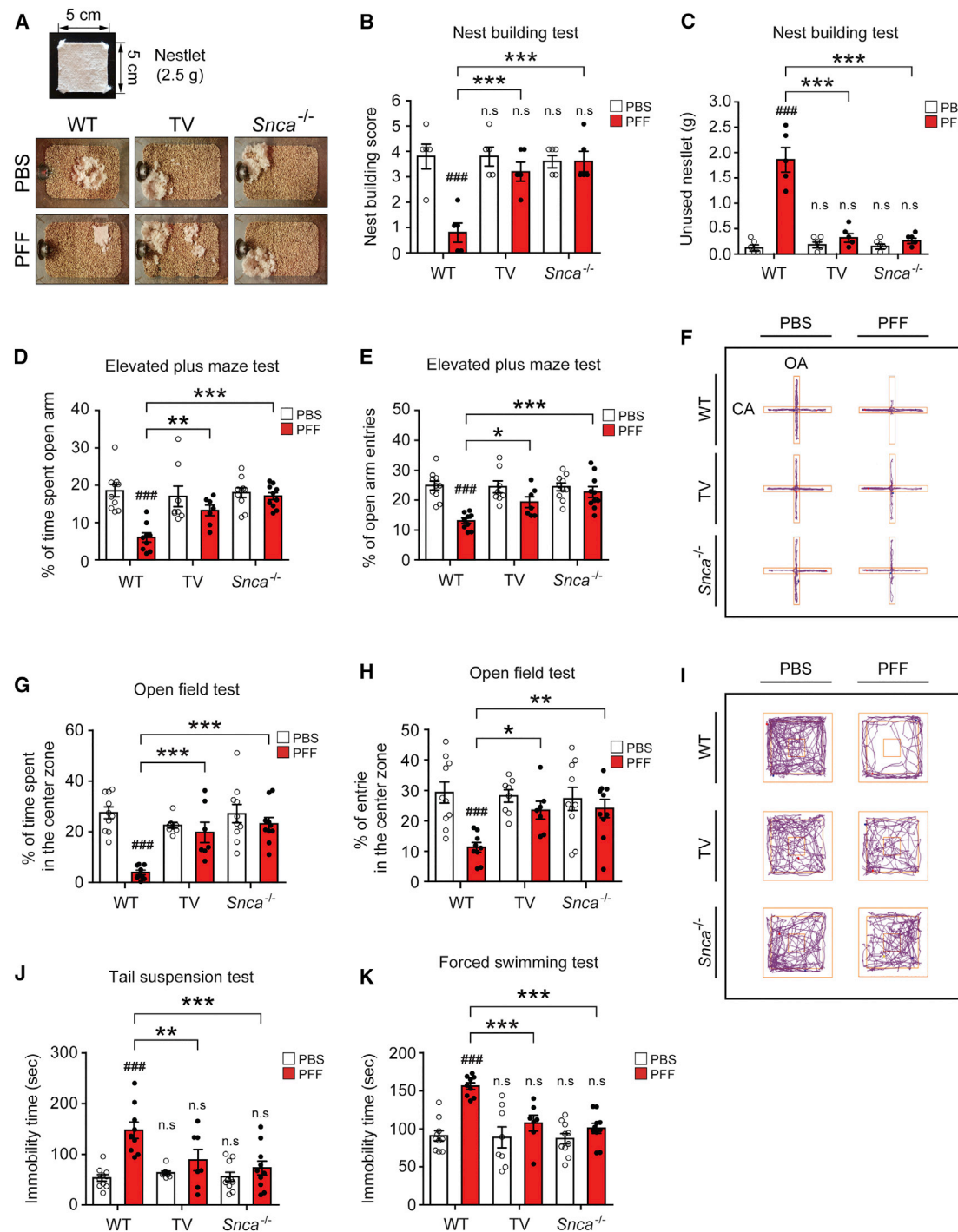


**Figure 5. Vagotomy and  $\alpha$ -syn Deficiency Prevent Deficits in Psychological Behavior Induced by  $\alpha$ -syn PFF Injection into the Gut**

Behavioral assessments of psychological behavior at 7 months after PBS and  $\alpha$ -syn PFF gastrointestinal injection were performed in WT (n = 9–10), TV (n = 7–8), and *Snca*<sup>-/-</sup> mice (n = 10).

(A) Representative images of nest building. Images show nest building after 16 h following introduction of nestlet in among all experimental groups.

(B and C) Nest building score (B) and unused nestlet (C) in the nest-building test. Nest-building scores were assessed, and the amount of unused nestlet material was measured after 16 h.

(D and E) Percentage of time spent in the open arm (D) and open arm entries (E) in the elevated plus maze (EPM).

(F) Representative movement paths of mice from each group in the EPM.

(legend continued on next page)

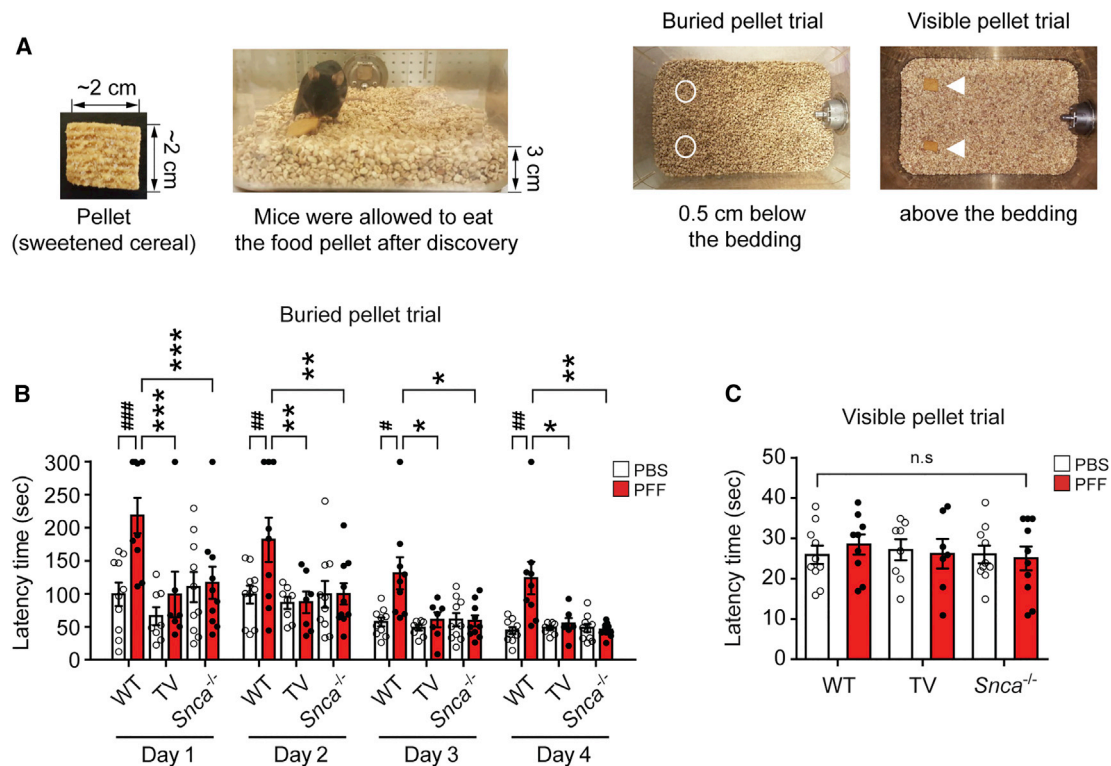


**Figure 6. Vagotomy and  $\alpha$ -syn Deficiency Prevent Olfactory Dysfunctions Induced by  $\alpha$ -syn PFF Injection into the Gut**

(A–C) Olfactory behavioral assessments at 9 months after PBS and  $\alpha$ -syn PFF gastrointestinal injection in WT (n = 9–10), TV (n = 7–8), and *Snca*<sup>-/-</sup> mice (n = 10). The buried pellet trial test was performed for 4 days, and the surface pellet control test was performed for one trial 1 day after the buried pellets.

(A) Two pieces of sweetened cereal were buried along the perimeter of the cage approximately 0.5 cm below the bedding so that it was not visible.

(B) Latency in finding the first pellet was recorded when the mouse touched the pellet.

(C) The visible pellet trial test was set up in a similar way except that the piece of cereal was placed on top of the bedding.

Error bars represent the mean  $\pm$  SEM. Statistical significance was determined using a two-way ANOVA followed by post hoc Bonferroni test for multiple group comparison. #p < 0.05; ##p < 0.01; ###p < 0.001 versus PBS gastrointestinal-injected WT group. \*p < 0.05; \*\*p < 0.01; \*\*\*p < 0.001 versus  $\alpha$ -syn PFF gastrointestinal-injected WT group, n.s., not significant.

gastrointestinal tract in a stereotypic manner via the vagus nerve into the brain. This work supports the Braak hypothesis. This approach also more closely models the clinical syndrome and manifestations of idiopathic PD, including both motor and non-motor symptoms. This approach also circumvents the concerns of injecting a pathologic protein directly into the brain.

Pathological  $\alpha$ -syn is closely correlated with PD and DLB (Forman et al., 2004). Interestingly,  $\alpha$ -syn pathology in PD is not limited to the brain and is also observed in the peripheral nervous system (PNS), including the ENS (Wakabayashi et al., 2010). More importantly,  $\alpha$ -syn aggregates have been detected in the ENS prior to any pathogenic changes in the CNS in  $\alpha$ -syn transgenic mice (Kuo et al., 2010), and other human studies have

shown that this is associated with increased intestinal permeability and translocation of bacteria and their products, resulting in oxidative stress (Forsyth et al., 2011). Recent studies on the gut microbiome suggested that short-chain fatty acids and extracellular fibers, such as curli, produced from microbes in the gastrointestinal tract could affect  $\alpha$ -syn aggregation and motor dysfunction (Chapman et al., 2002; Sampson et al., 2016). In addition, intragastric administration of rotenone in mice was capable of inducing oxidative stress and accumulation of phosphorylated  $\alpha$ -syn in the ENS and DMV, eventually resulting in neurodegeneration in the SNc (Pan-Montojo et al., 2010, 2012). Enteroendocrine cells in the gut epithelium, which face the lumen and are connected to enteric nerves, were discovered

(G and H) Effect of TV and  $\alpha$ -syn deficiency on  $\alpha$ -syn PFF-induced locomotion and central activity in the OFT. The data of percentage of (G) time spent and (H) entries in the center zone in the OFT are shown.

(I) Representative movement paths of mice from each group in the OFT.

(J and K) Effect of vagotomy and  $\alpha$ -syn deficiency on  $\alpha$ -syn PFF-induced depressive-like behavior in the (J) tail suspension test (TST) and (K) forced swimming test (FST). The immobility times were recorded using the video tracking system (Any-Maze software) during final 4 min of a total 6-min test.

Error bars represent the mean  $\pm$  SEM. All behavior tests were analyzed by two-way ANOVA followed by post hoc Bonferroni test for multiple group comparison. ###p < 0.001 versus PBS gastrointestinal-injected WT group. \*p < 0.05; \*\*p < 0.01; \*\*\*p < 0.001 versus  $\alpha$ -syn PFF gastrointestinal-injected WT group, n.s., not significant. See also Figure S6 and Videos S3, S4, and S5.

as a potential site through which various toxic substances can encounter  $\alpha$ -syn, ultimately leading to assembly and spread of pathological  $\alpha$ -syn to the myenteric plexus (Chandra et al., 2017). Taken together, these studies provide a potential mechanism for initiation of  $\alpha$ -syn pathology in the ENS consistent with Braak's hypothesis (Braak et al., 2007).

Braak and colleagues originally proposed that PD pathology may start in the digestive tract and spread from the gut to the brain via the vagus nerve (Braak et al., 2003a, 2004) and later suggested that "PD could be caused by a pathogen that enters the body via the nasal cavity and subsequently is swallowed and reaches the gut, initiating Lewy pathology in the nose and the digestive tract" to account for concurrent occurrence of Lewy pathology in the olfactory system and gastrointestinal (GI) tract (Hawkes et al., 2009). Our results support the theory that PD could begin in the gastrointestinal tract and spread through the vagus nerve to the brain because pSer129- $\alpha$ -syn immunoreactivity was observed in anatomically connected brain regions, such as the DMV, 1 month after  $\alpha$ -syn PFF injection into the duodenum and pylorus of the mouse stomach (Figures 1D–1F, S1D, and S2). This corresponds to Braak's stage 1. Three months after  $\alpha$ -syn PFF injection, pathological  $\alpha$ -syn is observed in the LC, amygdala, and hypothalamus, which are rostral sites anatomically interconnected with the MO (Figures 1D–1F, S1D, and S2). A small degree of pathological  $\alpha$ -syn was also detected in the SNc 3 months after  $\alpha$ -syn PFF injection (Figures 1D–1F, S1D, and S2). These sites correspond with Braak's stage 2–3. Later,  $\alpha$ -syn pathology further spreads into the STR, HIP, PFC, and OB at 7 months after  $\alpha$ -syn PFF injection, and the degree of pathological  $\alpha$ -syn was further increased in the STR, HIP, PFC, and OB 10 months after  $\alpha$ -syn PFF injection (Figures 1D–1F, S1D, and S2). These sites are considered to be consistent with Braak's later stages. Degeneration of DA neurons was observed in the SNc, and the levels of DA were reduced in the STR at 7 months (Figures 3 and S3). Interestingly, the degree of pathological  $\alpha$ -syn was slightly decreased in the DMV, LC, AMG, and SNc 10 months after  $\alpha$ -syn PFF injection when compared to the 7 months post-injection assessment of pathological  $\alpha$ -syn. These findings are consistent with prior observations that pathological  $\alpha$ -syn levels can plateau after  $\alpha$ -syn PFF injection (Manfredsson et al., 2018; Rey et al., 2016; Uemura et al., 2018). In a similar manner, seeded tauopathy can plateau after tau fibrils injection (Guo et al., 2016).

It is important to note that non-motor symptoms, such as hypospasmia, disturbances in sleep, gastrointestinal dysfunction, and cognitive and emotional deficits, are common features of clinical PD along with the motor symptoms (Pfeiffer, 2003; Ponsen et al., 2004; Ressler and Mayberg, 2007). Accordingly, we assessed a wide range of behavioral and gastrointestinal deficits in this model, in addition to the well-known motor deficits in PD. 7 months post-injection of  $\alpha$ -syn PFF, when there are reductions in DA, the mice performed poorly on the pole test, which is a sensitive DA motor test (Fleming et al., 2004; Taylor et al., 2010). Vagotomy or the absence of *Snca* prevented the pole test and grip strength deficits (Figures 3G and 3H). Interestingly, at the same time point, the reductions in DA did not affect swimming speed and distance in the water maze test (Figures S6A and S6B). The lack of an effect on swimming speed and distance

is consistent with the observation that reductions in striatal DA elicited by DA neurotoxins or DA transporter overexpression do not affect swimming speeds and distance (Bernhardt et al., 2018; Da Cunha et al., 2002; Miyoshi et al., 2002; Santiago et al., 2010; Sariñana and Tonegawa, 2016; Tadaiesky et al., 2008). A plausible explanation for these different motor function results is that PD patients move more easily in aquatic conditions, because it requires less balance than on land (Marinho-Buzelli et al., 2015). Moreover, it is known that some rodent behavioral tests appear to be much more sensitive to dopaminergic function than others. For instance, the pole test is sensitive to dopaminergic function and others are not (Fleming et al., 2004; Taylor et al., 2010), which is similar to the results reported here.

In addition to the motor deficits, injection of  $\alpha$ -syn PFF in the muscle layers of the pylorus and duodenum causes cognitive impairments, including memory and social deficits, anxiety, depression, and olfactory and gastrointestinal dysfunction (Figures 4, 5, 6, and S4). Although the underlying mechanistic details causing these deficits remain to be tested, it can be postulated that changes in the microbiota and gut-to-brain communication (Phelps et al., 2017; Villageliú et al., 2018), alterations in neurotransmitter systems (Chaudhuri and Schapira, 2009; Delaville et al., 2011; Mayeux, 1990) and growth factors (O'Leary et al., 2018), and perturbations in the immune system (Leonard and Myint, 2006) could play a pivotal role in the non-motor symptoms. Whether there is neuronal loss, the presence of pathologic  $\alpha$ -syn disrupts neuronal circuitry, or both contribute to these non-motor symptoms will require further study.

One point to consider is that the olfactory system is affected late in our model. PD is associated with early involvement of the gastrointestinal tract and the olfactory system, which are sites where endogenous  $\alpha$ -syn can be exposed to the external environment. It is likely that separate and combinatory processes of initiation via nasal and/or gastric routes and spread contribute to PD and DLB, and in some patients, there may be a dual hit (Hawkes et al., 2007). In any event, our model resulted in the olfactory dysfunction in the late stage, indicating that olfactory dysfunction can originate from processes that start in the gastrointestinal tract.

In cohort studies with follow-up from northern Europe, individuals who underwent truncal vagotomy had a lower risk for developing PD than age- and sex-matched control individuals (Liu et al., 2017; Svensson et al., 2015; Tysnes et al., 2015). Moreover, cervical vagotomy prior to inoculation of  $\alpha$ -syn PFF into the mouse gastric wall efficiently blocked the formation of  $\alpha$ -syn aggregates in the DMV (Uemura et al., 2018). Consistent with these results, we also observed that truncal vagotomy prior to  $\alpha$ -syn PFF injection into the muscle layers of the pylorus and duodenum prevented the spread of pathological  $\alpha$ -syn to the CNS and loss of dopaminergic neuron in the SNc and restored the levels of striatal DA and motor and non-motor symptoms, supporting that the vagus nerve is involved in the gut-to-brain axis as a route of transmission of pathological  $\alpha$ -syn (Figures 3, 4, 5, and 6). Also, selective expression of human  $\alpha$ -syn into the vagus nerve in the neck by injection of adeno-associated viral vector showed progressive spread of  $\alpha$ -syn aggregates from the MO to more rostral brain regions where axonal projections

innervate the MO (Ulusoy et al., 2013). Although our results showed that the stereotypical pattern of spread of pathological  $\alpha$ -syn is consistent with synaptically connected interneuronal transmission, LB pathology is not observed in all synaptically connected regions (Surmeier et al., 2017). Further investigation is needed to characterize which factors contribute to the selective vulnerability of neuronal systems to LB pathology.

Compared to previous reports regarding propagation from gut to brain, inoculation of  $\alpha$ -syn PFF or different forms of  $\alpha$ -syn (monomeric, oligomeric, and fibrillary) into the gastrointestinal tract showed that pathological  $\alpha$ -syn was able to reach the lower brainstem via the vagus nerve (Manfredsson et al., 2018; Uemura et al., 2018) or that  $\alpha$ -syn was capable of being transported via the vagal nerve (Holmqvist et al., 2014). However, pathological  $\alpha$ -syn did not spread to the rostral sites from the DMV and degree of pathological  $\alpha$ -syn declined over time in previous studies and eventually failed to elicit loss of dopaminergic neurons in the SNc and behavioral deficits observed in PD. It can be speculated that at least some of the different methodologies, including lower amounts and different forms of delivered pathological  $\alpha$ -syn, time after injection, and injection site, could produce different outcomes. In comparing our study to Manfredsson et al. (2018; Table S1), they injected a similar size of mouse  $\alpha$ -syn PFF but a smaller amount of  $\alpha$ -syn PFF per body weight (60  $\mu$ g/220 g of rat; 0.272  $\mu$ g of PFF per gram body weight) than the amount used in this study (25  $\mu$ g/25 g of mice; 1  $\mu$ g of PFF per gram body weight). Moreover, they injected  $\alpha$ -syn PFF into the descending colon, which is poorly innervated by the vagus nerve. Uemura et al. (2018) only injected mouse  $\alpha$ -syn PFF into the intestinal wall of the stomach and not the pylorus or duodenum. Although Uemura et al. (2018) injected higher amounts of  $\alpha$ -syn PFF (48  $\mu$ g/25 g of mice; 1.92  $\mu$ g of PFF per gram body weight), the size of  $\alpha$ -syn PFF was over 200 nm. It has been reported that the seeding activity of PFF is size dependent and that smaller size fibrils (<100 nm) transmit more readily than larger fibrils (Tarutani et al., 2016). Transmission electron microscopy (TEM) images of the  $\alpha$ -syn PFF used in this study (Figures S1B and S1C) indicate that the average size of our  $\alpha$ -syn PFF is 64.7 nm. In the Holmqvist study, they injected human brain lysates into mouse brain without substantial pathology (Holmqvist et al., 2014). Our preliminary studies comparing mouse and human  $\alpha$ -syn PFF (Figure S3) indicate that human  $\alpha$ -syn PFF is not as capable as mouse  $\alpha$ -syn PFF in spreading, which is consistent with the finding that mouse  $\alpha$ -syn PFF are substantially more effective than human  $\alpha$ -syn PFF in the intrastriatal mouse model (Luk et al., 2012). In summary, there are at least three key variables that are critical for successful gut-to-brain transmission of pathologic  $\alpha$ -syn: (1) location of injection (intestinal wall of the pyloric stomach and the duodenum); (2) average size of  $\alpha$ -syn PFF needs to be less than 100 nm in size; and (3) 1  $\mu$ g of PFF per gram body weight needs to be injected (Table S1).

Taken together, this study supports the Braak hypothesis of temporal and stereotypical spreading of LB pathology from gut to brain, leading to clinical features of idiopathic PD, including both motor and non-motor symptoms. This new model implicates the gut-brain axis in the etiology of idiopathic PD and will serve to accelerate the study of specific cellular and molecular

pathways associated with the centripetal trafficking of pathologic  $\alpha$ -syn from the gut to brain in PD and related  $\alpha$ -synucleinopathies and will help to test potential therapeutic interventions to mitigate risk of developing sporadic PD.

## STAR★METHODS

Detailed methods are provided in the online version of this paper and include the following:

- KEY RESOURCES TABLE
- LEAD CONTACT AND MATERIALS AVAILABILITY
- EXPERIMENTAL MODEL AND SUBJECT DETAILS
  - Animals
- METHOD DETAILS
  - $\alpha$ -Synuclein purification and  $\alpha$ -syn preformed fibrils (PFF) preparation
  - Intestinal intramuscular  $\alpha$ -syn PFF injection and vagotomy
  - Behavioral tests
  - Pole test
  - Rotarod test
  - Grip strength test
  - Spontaneous alternation behavior Y-maze test
  - Novel object recognition test (NORT)
  - Step-through passive avoidance test
  - Morris water maze test (MWM)
  - Nest building test (NBT)
  - Elevated plus maze (EPM)
  - Open field test (OFT)
  - Tail suspension test (TST)
  - Forced swimming test (FST)
  - Buried pellet test (BPT)
  - Single Photon Emission Computed Tomography-Computed Tomography (SPECT/CT) imaging in mice
  - Immunohistochemistry and quantitative analysis
  - Immunofluorescence analysis
  - Tissue lysate preparation
  - Immunoblot analysis
  - Assessments of body weight change, food intake, serum ghrelin levels, and fecal output
  - Monoamine analysis
- QUANTIFICATION AND STATISTICAL ANALYSIS
- DATA AND CODE AVAILABILITY

## SUPPLEMENTAL INFORMATION

Supplemental Information can be found online at <https://doi.org/10.1016/j.neuron.2019.05.035>.

## ACKNOWLEDGMENTS

We appreciate Taek-soo Lee, PhD, and Benjamin Tsui, PhD, technical assistance for SPECT-CT analysis. We thank I.-H. Wu for graphic art assistance. This work was supported by grants from the JPB Foundation, NIH/NINDS Morris K. Udall Parkinson's Disease Research Center NS38377, NIH/NINDS NS082205, NS10704, and NS098006 and NIH/NIA AG059686. The authors acknowledge the joint participation by the Adrienne Helis Malvin Medical Research Foundation through its direct engagement in the continuous active conduct of medical research in conjunction with the Johns Hopkins Hospital

and the Johns Hopkins University School of Medicine and the Foundation's Parkinson's Disease Program M-2014.

## AUTHOR CONTRIBUTIONS

S. Kim and S.-H.K. led the project and contributed to all aspects of the study. T.-I.K., N.P., S.L., W.R.K., M.K., and H.L. contributed to biochemical assay. S.S.K. contributed to HPLC analysis; J.H.L. and S. Kulkarni supported GI injection of PFF; C.A.F., C.S., and M.G.P. contributed to SPEC-CT analysis; P.J.P., G.L., V.L.D., T.M.D., and H.S.K. designed research; S. Kim S.-H.K., V.L.D., T.M.D., and H.S.K. analyzed data; and S. Kim, S.-H.K., V.L.D., T.M.D., and H.S.K. wrote the paper.

## DECLARATION OF INTERESTS

The authors declare no competing interests.

Received: July 24, 2018

Revised: April 3, 2019

Accepted: May 22, 2019

Published: June 26, 2019

## REFERENCES

- Anderson, J.P., Walker, D.E., Goldstein, J.M., de Laat, R., Banducci, K., Caccavello, R.J., Barbour, R., Huang, J., Kling, K., Lee, M., et al. (2006). Phosphorylation of Ser-129 is the dominant pathological modification of alpha-synuclein in familial and sporadic Lewy body disease. *J. Biol. Chem.* **281**, 29739–29752.
- Arias, N., Méndez, M., and Arias, J.L. (2015). The importance of the context in the hippocampus and brain related areas throughout the performance of a fear conditioning task. *Hippocampus* **25**, 1242–1249.
- Bernhardt, N., Lieser, M.K., Hlusicka, E.B., Habelt, B., Wieske, F., Edemann-Calleen, H., Garthe, A., and Winter, C. (2018). Learning deficits in rats overexpressing the dopamine transporter. *Sci. Rep.* **8**, 14173.
- Berthoud, H.R., Carlson, N.R., and Powley, T.L. (1991). Topography of efferent vagal innervation of the rat gastrointestinal tract. *Am. J. Physiol.* **260**, R200–R207.
- Bevins, R.A., and Besheer, J. (2006). Object recognition in rats and mice: a one-trial non-matching-to-sample learning task to study 'recognition memory'. *Nat. Protoc.* **1**, 1306–1311.
- Braak, H., Del Tredici, K., Rüb, U., de Vos, R.A., Jansen Steur, E.N., and Braak, E. (2003a). Staging of brain pathology related to sporadic Parkinson's disease. *Neurobiol. Aging* **24**, 197–211.
- Braak, H., Rüb, U., Gai, W.P., and Del Tredici, K. (2003b). Idiopathic Parkinson's disease: possible routes by which vulnerable neuronal types may be subject to neuroinvasion by an unknown pathogen. *J. Neural Transm. (Vienna)* **110**, 517–536.
- Braak, H., Ghebremedhin, E., Rüb, U., Bratzke, H., and Del Tredici, K. (2004). Stages in the development of Parkinson's disease-related pathology. *Cell Tissue Res.* **318**, 121–134.
- Braak, H., Sastre, M., Bohl, J.R., de Vos, R.A., and Del Tredici, K. (2007). Parkinson's disease: lesions in dorsal horn layer I, involvement of parasympathetic and sympathetic pre- and postganglionic neurons. *Acta Neuropathol.* **113**, 421–429.
- Calabresi, P., Picconi, B., Tozzi, A., Ghiglieri, V., and Di Filippo, M. (2014). Direct and indirect pathways of basal ganglia: a critical reappraisal. *Nat. Neurosci.* **17**, 1022–1030.
- Chandra, R., Hiniker, A., Kuo, Y.M., Nussbaum, R.L., and Liddle, R.A. (2017).  $\alpha$ -synuclein in gut endocrine cells and its implications for Parkinson's disease. *JCI Insight* **2**, 92295.
- Chapman, M.R., Robinson, L.S., Pinkner, J.S., Roth, R., Heuser, J., Hammar, M., Normark, S., and Hultgren, S.J. (2002). Role of *Escherichia coli* curli operons in directing amyloid fiber formation. *Science* **295**, 851–855.
- Chaudhuri, K.R., and Schapira, A.H. (2009). Non-motor symptoms of Parkinson's disease: dopaminergic pathophysiology and treatment. *Lancet Neurol.* **8**, 464–474.
- Cryan, J.F., Mombereau, C., and Vassout, A. (2005). The tail suspension test as a model for assessing antidepressant activity: review of pharmacological and genetic studies in mice. *Neurosci. Biobehav. Rev.* **29**, 571–625.
- Da Cunha, C., Angelucci, M.E., Canteras, N.S., Wonnacott, S., and Takahashi, R.N. (2002). The lesion of the rat substantia nigra pars compacta dopaminergic neurons as a model for Parkinson's disease memory disabilities. *Cell. Mol. Neurobiol.* **22**, 227–237.
- Deacon, R.M. (2006). Assessing nest building in mice. *Nat. Protoc.* **1**, 1117–1119.
- Delaville, C., Deurwaerdère, P.D., and Benazzouz, A. (2011). Noradrenaline and Parkinson's disease. *Front. Syst. Neurosci.* **5**, 31.
- Dodel, R., Csoti, I., Ebersbach, G., Fuchs, G., Hahne, M., Kuhn, W., Oechsner, M., Jost, W., Reichmann, H., and Schulz, J.B. (2008). Lewy body dementia and Parkinson's disease with dementia. *J. Neurol.* **255** (Suppl 5), 39–47.
- Eagle, A.L., Wang, H., and Robison, A.J. (2016). Sensitive assessment of hippocampal learning using temporally dissociated passive avoidance task. *Biol. Protoc.* **6**, e1821.
- El-Salhy, M., Danielsson, A., Axelsson, H., and Qian, B.F. (2000). Neuroendocrine peptide levels in the gastrointestinal tract of mice after unilateral cervical vagotomy. *Regul. Pept.* **88**, 15–20.
- Fleming, S.M., Salcedo, J., Fernagut, P.O., Rockenstein, E., Masliah, E., Levine, M.S., and Chesselet, M.F. (2004). Early and progressive sensorimotor anomalies in mice overexpressing wild-type human alpha-synuclein. *J. Neurosci.* **24**, 9434–9440.
- Fleming, S.M., Tetreault, N.A., Mulligan, C.K., Hutson, C.B., Masliah, E., and Chesselet, M.F. (2008). Olfactory deficits in mice overexpressing human wild-type alpha-synuclein. *Eur. J. Neurosci.* **28**, 247–256.
- Forman, M.S., Trojanowski, J.Q., and Lee, V.M. (2004). Neurodegenerative diseases: a decade of discoveries paves the way for therapeutic breakthroughs. *Nat. Med.* **10**, 1055–1063.
- Forsyth, C.B., Shannon, K.M., Kordower, J.H., Voigt, R.M., Shaikh, M., Jaglin, J.A., Estes, J.D., Dodiya, H.B., and Keshavarzian, A. (2011). Increased intestinal permeability correlates with sigmoid mucosa alpha-synuclein staining and endotoxin exposure markers in early Parkinson's disease. *PLoS ONE* **6**, e28032.
- Fujiwara, H., Hasegawa, M., Dohmae, N., Kawashima, A., Masliah, E., Goldberg, M.S., Shen, J., Takio, K., and Iwatsubo, T. (2002). alpha-synuclein is phosphorylated in synucleinopathy lesions. *Nat. Cell Biol.* **4**, 160–164.
- Furness, J.B. (2012). The enteric nervous system and neurogastroenterology. *Nat. Rev. Gastroenterol. Hepatol.* **9**, 286–294.
- Gelpi, E., Navarro-Otano, J., Tolosa, E., Gaig, C., Compta, Y., Rey, M.J., Martí, M.J., Hernández, I., Valldeoriola, F., Reñé, R., and Ribalta, T. (2014). Multiple organ involvement by alpha-synuclein pathology in Lewy body disorders. *Mov. Disord.* **29**, 1010–1018.
- Guo, J.L., Narasimhan, S., Changolkar, L., He, Z., Stieber, A., Zhang, B., Gathagan, R.J., Iba, M., McBride, J.D., Trojanowski, J.Q., and Lee, V.M. (2016). Unique pathological tau conformers from Alzheimer's brains transmit tau pathology in nontransgenic mice. *J. Exp. Med.* **213**, 2635–2654.
- Hawkes, C.H., Del Tredici, K., and Braak, H. (2007). Parkinson's disease: a dual-hit hypothesis. *Neuropathol. Appl. Neurobiol.* **33**, 599–614.
- Hawkes, C.H., Del Tredici, K., and Braak, H. (2009). Parkinson's disease: the dual hit theory revisited. *Ann. N Y Acad. Sci.* **1170**, 615–622.
- Holmqvist, S., Chutna, O., Bousset, L., Aldrin-Kirk, P., Li, W., Björklund, T., Wang, Z.Y., Roybon, L., Melki, R., and Li, J.Y. (2014). Direct evidence of Parkinson pathology spread from the gastrointestinal tract to the brain in rats. *Acta Neuropathol.* **128**, 805–820.
- Karpowicz, R.J., Jr., Trojanowski, J.Q., and Lee, V.M. (2019). Transmission of  $\alpha$ -synuclein seeds in neurodegenerative disease: recent developments. *Lab. Invest.* Published online February 13, 2019. <https://doi.org/10.1038/s41374-019-0195-z>.

- Karuppagounder, S.S., Brahmachari, S., Lee, Y., Dawson, V.L., Dawson, T.M., and Ko, H.S. (2014). The c-Abl inhibitor, nilotinib, protects dopaminergic neurons in a preclinical animal model of Parkinson's disease. *Sci. Rep.* 4, 4874.
- Klingelhofer, L., and Reichmann, H. (2015). Pathogenesis of Parkinson disease—the gut-brain axis and environmental factors. *Nat. Rev. Neurol.* 11, 625–636.
- Kuo, Y.M., Li, Z., Jiao, Y., Gaborit, N., Pani, A.K., Orrison, B.M., Bruneau, B.G., Giasson, B.I., Smeyne, R.J., Gershon, M.D., and Nussbaum, R.L. (2010). Extensive enteric nervous system abnormalities in mice transgenic for artificial chromosomes containing Parkinson disease-associated alpha-synuclein gene mutations precede central nervous system changes. *Hum. Mol. Genet.* 19, 1633–1650.
- Kwon, S.H., Kim, H.C., Lee, S.Y., and Jang, C.G. (2009). Loganiin improves learning and memory impairments induced by scopolamine in mice. *Eur. J. Pharmacol.* 619, 44–49.
- Lee, S.J., Desplats, P., Sigurdson, C., Tsigelny, I., and Masliah, E. (2010). Cell-to-cell transmission of non-prion protein aggregates. *Nat. Rev. Neurol.* 6, 702–706.
- Leonard, B.E., and Myint, A. (2006). Changes in the immune system in depression and dementia: causal or coincidental effects? *Dialogues Clin. Neurosci.* 8, 163–174.
- Liu, B., Fang, F., Pedersen, N.L., Tillander, A., Ludvigsson, J.F., Ekblom, A., Svenningsson, P., Chen, H., and Wirdefeldt, K. (2017). Vagotomy and Parkinson disease: a Swedish register-based matched-cohort study. *Neurology* 88, 1996–2002.
- Luk, K.C., Song, C., O'Brien, P., Stieber, A., Branch, J.R., Brunden, K.R., Trojanowski, J.Q., and Lee, V.M. (2009). Exogenous alpha-synuclein fibrils seed the formation of Lewy body-like intracellular inclusions in cultured cells. *Proc. Natl. Acad. Sci. USA* 106, 20051–20056.
- Luk, K.C., Kehm, V., Carroll, J., Zhang, B., O'Brien, P., Trojanowski, J.Q., and Lee, V.M. (2012). Pathological  $\alpha$ -synuclein transmission initiates Parkinson-like neurodegeneration in nontransgenic mice. *Science* 338, 949–953.
- Manfredsson, F.P., Luk, K.C., Benskey, M.J., Gezer, A., Garcia, J., Kuhn, N.C., Sandoval, I.M., Patterson, J.R., O'Mara, A., Yonkers, R., and Kordower, J.H. (2018). Induction of alpha-synuclein pathology in the enteric nervous system of the rat and non-human primate results in gastrointestinal dysmotility and transient CNS pathology. *Neurobiol. Dis.* 112, 106–118.
- Mao, X., Ou, M.T., Karuppagounder, S.S., Kam, T.I., Yin, X., Xiong, Y., Ge, P., Umanah, G.E., Brahmachari, S., Shin, J.H., et al. (2016). Pathological  $\alpha$ -synuclein transmission initiated by binding lymphocyte-activation gene 3. *Science* 353, aah3374.
- Marinho-Buzelli, A.R., Bonnyman, A.M., and Verrier, M.C. (2015). The effects of aquatic therapy on mobility of individuals with neurological diseases: a systematic review. *Clin. Rehabil.* 29, 741–751.
- Mayeux, R. (1990). The "serotonin hypothesis" for depression in Parkinson's disease. *Adv. Neurol.* 53, 163–166.
- Miyoshi, E., Wietzikoski, S., Camplesse, M., Silveira, R., Takahashi, R.N., and Da Cunha, C. (2002). Impaired learning in a spatial working memory version and in a cued version of the water maze in rats with MPTP-induced mesencephalic dopaminergic lesions. *Brain Res. Bull.* 58, 41–47.
- O'Leary, O.F., Ogbonnaya, E.S., Felice, D., Levone, B.R., C Conroy, L., Fitzgerald, P., Bravo, J.A., Forsythe, P., Bienenstock, J., Dinan, T.G., and Cryan, J.F. (2018). The vagus nerve modulates BDNF expression and neurogenesis in the hippocampus. *Eur. Neuropsychopharmacol.* 28, 307–316.
- Pan-Montojo, F., Anichtchik, O., Dening, Y., Knels, L., Pursche, S., Jung, R., Jackson, S., Gille, G., Spillantini, M.G., Reichmann, H., and Funk, R.H. (2010). Progression of Parkinson's disease pathology is reproduced by intragastric administration of rotenone in mice. *PLoS ONE* 5, e8762.
- Pan-Montojo, F., Schwarz, M., Winkler, C., Arnhold, M., O'Sullivan, G.A., Pal, A., Said, J., Marsico, G., Verbavatz, J.M., Rodrigo-Angulo, M., et al. (2012). Environmental toxins trigger PD-like progression via increased alpha-synuclein release from enteric neurons in mice. *Sci. Rep.* 2, 898.
- Pellow, S., and File, S.E. (1986). Anxiolytic and anxiogenic drug effects on exploratory activity in an elevated plus-maze: a novel test of anxiety in the rat. *Pharmacol. Biochem. Behav.* 24, 525–529.
- Pfeiffer, R.F. (2003). Gastrointestinal dysfunction in Parkinson's disease. *Lancet Neurol.* 2, 107–116.
- Phelps, D., Brinkman, N.E., Keely, S.P., Anneken, E.M., Catron, T.R., Betancourt, D., Wood, C.E., Espenschied, S.T., Rawls, J.F., and Tal, T. (2017). Microbial colonization is required for normal neurobehavioral development in zebrafish. *Sci. Rep.* 7, 11244.
- Ponsen, M.M., Stoffers, D., Booi, J., van Eck-Smit, B.L., Wolters, E.Ch., and Berendse, H.W. (2004). Idiopathic hyposmia as a preclinical sign of Parkinson's disease. *Ann. Neurol.* 56, 173–181.
- Porsolt, R.D., Anton, G., Blavet, N., and Jalfre, M. (1978). Behavioural despair in rats: a new model sensitive to antidepressant treatments. *Eur. J. Pharmacol.* 47, 379–391.
- Ressler, K.J., and Mayberg, H.S. (2007). Targeting abnormal neural circuits in mood and anxiety disorders: from the laboratory to the clinic. *Nat. Neurosci.* 10, 1116–1124.
- Rey, N.L., Steiner, J.A., Maroof, N., Luk, K.C., Madaj, Z., Trojanowski, J.Q., Lee, V.M., and Brundin, P. (2016). Widespread transneuronal propagation of  $\alpha$ -synucleinopathy triggered in olfactory bulb mimics prodromal Parkinson's disease. *J. Exp. Med.* 213, 1759–1778.
- Rogers, R.C., Kita, H., Butcher, L.L., and Novin, D. (1980). Afferent projections to the dorsal motor nucleus of the vagus. *Brain Res. Bull.* 5, 365–373.
- Sakata, K., Jin, L., and Jha, S. (2010). Lack of promoter IV-driven BDNF transcription results in depression-like behavior. *Genes Brain Behav.* 9, 712–721.
- Sampson, T.R., Debelius, J.W., Thron, T., Janssen, S., Shastri, G.G., Ilhan, Z.E., Challis, C., Schretter, C.E., Rocha, S., Gradinaru, V., et al. (2016). Gut microbiota regulate motor deficits and neuroinflammation in a model of Parkinson's disease. *Cell* 167, 1469–1480.e12.
- Santiago, R.M., Barbiero, J., Lima, M.M., Dombrowski, P.A., Andreatini, R., and Vital, M.A. (2010). Depressive-like behaviors alterations induced by intranigral MPTP, 6-OHDA, LPS and rotenone models of Parkinson's disease are predominantly associated with serotonin and dopamine. *Prog. Neuropsychopharmacol. Biol. Psychiatry* 34, 1104–1114.
- Sariñana, J., and Tonegawa, S. (2016). Differentiation of forebrain and hippocampal dopamine 1-class receptors, D1R and D5R, in spatial learning and memory. *Hippocampus* 26, 76–86.
- Song, N., Liu, J., Shaheen, S., Du, L., Proctor, M., Roman, J., and Yu, J. (2015). Vagotomy attenuates bleomycin-induced pulmonary fibrosis in mice. *Sci. Rep.* 5, 13419.
- Song, N., Wang, W., Jia, F., Du, X., Xie, A., He, Q., Shen, X., Zhang, J., Rogers, J.T., Xie, J., and Jiang, H. (2017). Assessments of plasma ghrelin levels in the early stages of Parkinson's disease. *Mov. Disord.* 32, 1487–1491.
- Steru, L., Chermat, R., Thierry, B., and Simon, P. (1985). The tail suspension test: a new method for screening antidepressants in mice. *Psychopharmacology (Berl.)* 85, 367–370.
- Surmeier, D.J., Obeso, J.A., and Halliday, G.M. (2017). Selective neuronal vulnerability in Parkinson disease. *Nat. Rev. Neurosci.* 18, 101–113.
- Svensson, E., Horváth-Puhó, E., Thomsen, R.W., Djurhuus, J.C., Pedersen, L., Borghammer, P., and Sørensen, H.T. (2015). Vagotomy and subsequent risk of Parkinson's disease. *Ann. Neurol.* 78, 522–529.
- Tadaiesky, M.T., Dombrowski, P.A., Figueiredo, C.P., Cargnin-Ferreira, E., Da Cunha, C., and Takahashi, R.N. (2008). Emotional, cognitive and neurochemical alterations in a premotor stage model of Parkinson's disease. *Neuroscience* 156, 830–840.
- Talaga, A.K., Dong, F.N., Reisert, J., and Zhao, H. (2017). Cilia- and flagella-associated protein 69 regulates olfactory transduction kinetics in mice. *J. Neurosci.* 37, 5699–5710.
- Tarutani, A., Suzuki, G., Shimozaawa, A., Nonaka, T., Akiyama, H., Hisanaga, S., and Hasegawa, M. (2016). The effect of fragmented pathogenic  $\alpha$ -synuclein seeds on prion-like propagation. *J. Biol. Chem.* 291, 18675–18688.

- Taylor, T.N., Greene, J.G., and Miller, G.W. (2010). Behavioral phenotyping of mouse models of Parkinson's disease. *Behav. Brain Res.* *211*, 1–10.
- Ter Horst, G.J., Toes, G.J., and Van Willigen, J.D. (1991). Locus coeruleus projections to the dorsal motor vagus nucleus in the rat. *Neuroscience* *45*, 153–160.
- Tysnes, O.B., Kenborg, L., Herlofson, K., Steding-Jessen, M., Horn, A., Olsen, J.H., and Reichmann, H. (2015). Does vagotomy reduce the risk of Parkinson's disease? *Ann. Neurol.* *78*, 1011–1012.
- Uemura, N., Yagi, H., Uemura, M.T., Hatanaka, Y., Yamakado, H., and Takahashi, R. (2018). Inoculation of  $\alpha$ -synuclein preformed fibrils into the mouse gastrointestinal tract induces Lewy body-like aggregates in the brainstem via the vagus nerve. *Mol. Neurodegener.* *13*, 21.
- Ulusoy, A., Rusconi, R., Pérez-Revuelta, B.I., Musgrove, R.E., Helwig, M., Winzen-Reichert, B., and Di Monte, D.A. (2013). Caudo-rostral brain spreading of  $\alpha$ -synuclein through vagal connections. *EMBO Mol. Med.* *5*, 1119–1127.
- Villageliú, D.N., Rasmussen, S., and Lyte, M. (2018). A microbial endocrinology-based simulated small intestinal medium for the evaluation of neurochemical production by gut microbiota. *FEMS Microbiol. Ecol.* *94*, fty096.
- Volpicelli-Daley, L.A., Luk, K.C., Patel, T.P., Tanik, S.A., Riddle, D.M., Stieber, A., Meaney, D.F., Trojanowski, J.Q., and Lee, V.M. (2011). Exogenous  $\alpha$ -synuclein fibrils induce Lewy body pathology leading to synaptic dysfunction and neuron death. *Neuron* *72*, 57–71.
- Volpicelli-Daley, L.A., Luk, K.C., and Lee, V.M. (2014). Addition of exogenous  $\alpha$ -synuclein preformed fibrils to primary neuronal cultures to seed recruitment of endogenous  $\alpha$ -synuclein to Lewy body and Lewy neurite-like aggregates. *Nat. Protoc.* *9*, 2135–2146.
- Vorhees, C.V., and Williams, M.T. (2006). Morris water maze: procedures for assessing spatial and related forms of learning and memory. *Nat. Protoc.* *1*, 848–858.
- Wakabayashi, K., Mori, F., Tanji, K., Orimo, S., and Takahashi, H. (2010). Involvement of the peripheral nervous system in synucleinopathies, tauopathies and other neurodegenerative proteinopathies of the brain. *Acta Neuropathol.* *120*, 1–12.
- Watabe-Uchida, M., Zhu, L., Ogawa, S.K., Vamanrao, A., and Uchida, N. (2012). Whole-brain mapping of direct inputs to midbrain dopamine neurons. *Neuron* *74*, 858–873.
- Williams, D.L., Grill, H.J., Cummings, D.E., and Kaplan, J.M. (2003). Vagotomy dissociates short- and long-term controls of circulating ghrelin. *Endocrinology* *144*, 5184–5187.
- Wu, C.C., Lien, C.C., Hou, W.H., Chiang, P.M., and Tsai, K.J. (2016). Gain of BDNF function in engrafted neural stem cells promotes the therapeutic potential for Alzheimer's disease. *Sci. Rep.* *6*, 27358.

## STAR★METHODS

### KEY RESOURCES TABLE

REAGENT or RESOURCE	SOURCE	IDENTIFIER
<b>Antibodies</b>		
Mouse anti- $\alpha$ -Synuclein	BD Bioscience	Cat#610787; RRID: AB_398108
Mouse anti-pSer129- $\alpha$ -synuclein	Biolegend	Cat#825701; RRID: AB_2564891
Rabbit anti-pSer129- $\alpha$ -synuclein	Abcam	Cat#ab168381; RRID: AB_2728613
Rabbit anti-Tyrosine Hydroxylase (TH)	Novus Biologicals	Cat#NB300-109; RRID: AB_10077691
Rabbit anti-Dopamine transporter (DAT)	Sigma	Cat#D6944; RRID: AB_1840807
Rabbit anti-Tuj1	Biolegend	Cat#802001; RRID: AB_2564645
Rabbit anti-Choline Acetyltransferase (ChAT)	Abcam	Cat#Ab178850; RRID: AB_2721842
Mouse Anti-NeuN, clone A60, Cy3 Conjugate	Millipore	Cat#MAB377C3; RRID: AB_10918200
Mouse anti- $\beta$ -actin-HRP	Sigma	Cat#A3854; RRID: AB_262011
Donkey Anti-Rabbit IgG, Whole Ab ECL Antibody, HRP Conjugated	GE Healthcare	Cat#NA934; RRID: AB_772206
Sheep Anti-Mouse IgG, Whole Ab ECL Antibody, HRP Conjugated	GE Healthcare	Cat#NA931; RRID: AB_772210
Donkey polyclonal anti-mouse Alexa fluor 488	Jackson ImmunoResearch	Cat#715-545-151; RRID: AB_2341099
Donkey polyclonal anti-rabbit Alexa fluor 488	Jackson ImmunoResearch	Cat#711-545-152; RRID: AB_2313584
Donkey polyclonal anti-mouse CY3	Jackson ImmunoResearch	Cat#715-165-151; RRID: AB_2315777
Donkey polyclonal anti-rabbit CY3	Jackson ImmunoResearch	Cat#711-165-152; RRID: AB_2307443
<b>Chemicals, Peptides, and Recombinant Proteins</b>		
1X PBS pH 7.4	Quality Biologicals	Cat#114-058-101
10X TBS pH 7.4	Quality Biologicals	Cat#351-086-101
Protease Inhibitor Cocktail	Sigma	Cat#P8340
Phosphatase inhibitor cocktail 2	Sigma	Cat#P5726
Phosphatase inhibitor cocktail 3	Sigma	Cat#P0044
Paraformaldehyde (PFA) reagent grade	Sigma	Cat#P6148
D.P.X.	Sigma	Cat#317616
Thionin acetate salt	Sigma	Cat#T7029
Normal donkey serum	Jackson ImmunoResearch	Cat#017-000-121
VECTASHIELD HardSet Antifade Mounting Medium with DAPI	Vector laboratories	Cat#H-1500
SIGMAFAST(TM) 3,3'-Diaminobenzidine tablets	Sigma	Cat#D4293
[ <sup>123</sup> I]ioflupane	Cardinal Health	DaTScan
<b>Critical Commercial Assays</b>		
Vectastain Elite ABC Kit (Peroxidase, Rabbit IgG)	Vector laboratories	Cat#PK-6101
Vectastain Elite ABC Kit (Peroxidase, Mouse IgG)	Vector laboratories	Cat#PK-6102
Pierce LAL chromogenic endotoxin quantitation kit	Thermo Scientific	Cat#88282
Ghrelin (Rat, Mouse) EIA Kit, extraction-free	Phoenix Pharmaceuticals	Cat#EK-031-31
PIERCE BCA PROTEIN ASSAY	Thermo Scientific	Cat#23227
DreamTaq Green PCR Master Mix (2X)	Thermo Scientific	Cat#K1082
<b>Experimental Models: Organisms/Strains</b>		
Mouse: B6;129X1-Snca <sup>tm1Rosl</sup> /J	Jackson Laboratory	JAX:003692
Mouse: C57BL/6J	Jackson Laboratory	JAX:000664

(Continued on next page)

## Continued

REAGENT or RESOURCE	SOURCE	IDENTIFIER
<b>Oligonucleotides</b>		
Primer: Mouse SNCA wild type forward: 5'-GGC GAC GTG AAG GAG CCA GGG A -3'	Jackson Laboratory	oIMR1286
Primer: Mouse SNCA wild type reverse: 5'-CAG CGA AAG GAA AGC CGA GTG ATG TAC T-3'	Jackson Laboratory	oIMR1287
Primer: Mouse SNCA mutant forward: 5'-CTG AAT GAA CTG CAG GAC GA-3'	Jackson Laboratory	oIMR158
Primer: Mouse SNCA mutant reverse: 5'-ATA CTT TCT CGG CAG GAG CA-3'	Jackson Laboratory	oIMR159
<b>Recombinant DNA</b>		
pRK172-mouse $\alpha$ -Synuclein	<a href="#">Volpicelli-Daley et al., 2014</a>	N/A
pRK172-human $\alpha$ -Synuclein	<a href="#">Volpicelli-Daley et al., 2014</a>	N/A
<b>Deposited Data</b>		
Raw data used for this study	This manuscript	<a href="https://dx.doi.org/10.17632/swzrgbp3p5.1">https://dx.doi.org/10.17632/swzrgbp3p5.1</a>
<b>Software and Algorithms</b>		
ImageJ	NIH	<a href="https://imagej.nih.gov/ij/">https://imagej.nih.gov/ij/</a>
Prism 6	GraphPad software	<a href="https://www.graphpad.com/scientific-software/prism/">https://www.graphpad.com/scientific-software/prism/</a>
ZEN lite	Zeiss	<a href="https://www.zeiss.com/microscopy/us/products/microscope-software/zen.html">https://www.zeiss.com/microscopy/us/products/microscope-software/zen.html</a>
Stereo Investigator software	MBF Bioscience	<a href="https://www.mbfbioscience.com">https://www.mbfbioscience.com</a>
ML-EM algorithm	MI Labs	reconstruction
AMIDE	SOURCEFORGE	<a href="http://amide.sourceforge.net/">http://amide.sourceforge.net/</a>
ANY-maze	Stoelting Co.	<a href="https://www.stoeltingco.com/anymaze.html">https://www.stoeltingco.com/anymaze.html</a>
<b>Other</b>		
RIPA Lysis and Extraction Buffer	Thermo Scientific	Cat#89901
2X Lamml Sample Buffer	Bio-Rad	Cat#1610737
Novex WedgeWell 8-16% Tris-Glycine Mini Gels	Thermo Scientific	Cat#XP08165BOX
SUPER SIGNAL WEST PICO PLUS	Thermo Scientific	Cat#34580
Blotting-Grade Blocker, nonfat dry milk	Bio-Rad	Cat#1706404
Restore western blot stripping buffer	Thermo Scientific	Cat#21059
Nitrocellulose Membrane	Bio-Rad	Cat#1620115
X-ray film	RPI	Cat#248300
Hamilton GASTIGHT syringe, 1700 series	Sigma	Cat#20972
Pierce High Capacity Endotoxin Removal Spin Column	Thermo Scientific	Cat#88276
Superdex 200 Increase 10/300 G	GE Healthcare	Cat#45-002-570
Hitrap Q Sepharose Fast Flow	GE Healthcare	Cat#450-002-58
Ni Sepharose 6 Fast Flow	GE Healthcare	Cat#17-5318-06

## LEAD CONTACT AND MATERIALS AVAILABILITY

Further information and requests for resources and reagents should be directed to and will be fulfilled by the Lead Contact, Ted M. Dawson ([tdawson@jhmi.edu](mailto:tdawson@jhmi.edu)). There are no restrictions on any data or materials presented in this paper.

## EXPERIMENTAL MODEL AND SUBJECT DETAILS

### Animals

All experimental procedures were according to the guidelines of Laboratory Animal Manual of the National Institute of Health Guide to the Care and Use of Animals and were approved by the Johns Hopkins Medical Institute Animal Care and Use Committee. Animals were housed in a 12 h dark/light cycle with free access to water and food. Randomized mixed-gender cohorts were used for all animal

experiments. All mice were acclimatized for 3 days in the procedure room before any experiments were started. We have taken great effort to reduce animal suffering from pain and discomfort. C57BL/6J mice and  $\alpha$ -synuclein knockout (*Snca*<sup>-/-</sup>; B6;129X1-*Snca*<sup>tm1Rosl/J</sup>, Jackson Laboratory stock: 003692) mice were obtained from the Jackson Laboratories (ME, USA). Mice were mated with C57BL/6J mice for the present study.

For genotyping, the PCR reaction was performed using Veriti thermal cycler (Applied Biosystems), with the following PCR conditions: 94°C for 2 min as the first step; 10 cycles of 95°C for 20 s, 65°C for 15 s, and 68°C for 10 s as the second step; 28 cycles of 94°C for 15 s, 60°C for 15 s, 72°C for 10 s as the third step followed by 72°C for 1 min. Primer sequences used for the PCR were as follows: wild-type (WT) forward, 5'-GGC GAC GTG AAG GAG CCA GGG A -3'; WT reverse, 5'-CAG CGA AAG GAA AGC CGA GTG ATG TAC T-3'; mutant forward, 5'-CTG AAT GAA CTG CAG GAC GA-3'; mutant reverse, 5'-ATA CTT TCT CGG CAG GAG CA-3'. PCR product size for the WT was approximately 320 bp. For mutant, the PCR product size was approximately 172 bp. PCR products were subjected to 2% agarose gel electrophoresis to determine the genotype of mice.

## METHOD DETAILS

### $\alpha$ -Synuclein purification and $\alpha$ -syn preformed fibrils (PFF) preparation

Mouse and human recombinant full-length  $\alpha$ -synuclein protein were purified as previously described with IPTG independent inducible pRK172 vector system (Volpicelli-Daley et al., 2014). Briefly, bacteria were harvested by centrifugation at 6,000 x g for 10 min after 16 h incubation at 37°C. The bacterial pellet was resuspended in high salt buffer containing 10 mM Tris (pH 7.6), 750 mM NaCl, and 1 mM EDTA with complete protease inhibitor mixture (Sigma-Aldrich) and 1 mM PMSF, and lysed by sonicating for 5 min (30 s pulse on/off) at 60% amplitude (Branson Digital sonifier, Danbury, CT, USA) with boiling for 15 min. After centrifugation at 6,000 x g for 20 min, the supernatant was subjected to serial purification steps using Superdex 200 Increase 10/300 G size-exclusion and Hitrap Q Sepharose Fast Flow anion-exchange columns (GE Healthcare, Pittsburgh, PA, USA). Purified  $\alpha$ -syn was applied to High capacity endotoxin removal spin columns (Pierce, Rockford, IL, USA) and Ni Sepharose 6 Fast Flow (GE Healthcare) to remove endotoxin, followed by confirmation of removal of endotoxin using LAL Chromogenic Endotoxin Quantitation Kit (Pierce).  $\alpha$ -syn monomer was stored at -80°C until used.  $\alpha$ -syn PFF was prepared in PBS from 5 mg/ml of  $\alpha$ -syn monomer by stirring with magnetic stirrer (1,000 rpm at 37°C) for 1 week.  $\alpha$ -syn aggregates were sonicated for 30 s (0.5 s pulse on/off) at 10% amplitude (Branson Digital sonifier). To determine the length of  $\alpha$ -syn PFF,  $\alpha$ -syn PFF after sonication was imaged by transmission electron microscopy (TEM). Sonicated  $\alpha$ -syn PFF was adsorbed to glow discharge 400 mesh carbon-coated copper grids (EMS) for 2 min and rinsed with three drops of Tris-HCl (50 mM, pH7.4). The rinsed grids were floated upon two consecutive drops of 0.75% uranyl formate for 30 s each. Grids were allowed to dry before imaging on a Phillips CM 120 TEM (80 kV) with an AMT ER-80 charge-coupled device (8 megapixel). Images were captured and digitized by Philips EM 410 TEM with a Soft Imaging System Megaview III digital camera.

### Intestinal intramuscular $\alpha$ -syn PFF injection and vagotomy

Mice at 3 months of age were anesthetized using isoflurane (2%–4%) and kept at a constant body temperature using a conventional heat pad. Figure S1A provides a schematic of how the gastrointestinal  $\alpha$ -syn PFF injection experiment was performed. For each animal, the injection was conducted using a 10  $\mu$ L Hamilton syringe into the wall of the pyloric stomach at 2 sites and intestine wall of the duodenum at 2 sites, 0.5 cm apart from the pyloric stomach injection site. Injections were made near the myenteric plexus. The pyloric stomach was injected with 6.25  $\mu$ g  $\alpha$ -syn PFF in two different locations (2.5  $\mu$ g/ $\mu$ L, 2.5  $\mu$ L/location) for a total of 12.5  $\mu$ g  $\alpha$ -syn PFF, and the upper duodenum was injected with 6.25  $\mu$ g  $\alpha$ -syn PFF in two different locations (2.5  $\mu$ g/ $\mu$ L, total 2.5  $\mu$ L/location) for a total of 12.5  $\mu$ g  $\alpha$ -syn PFF. In addition, control mice were injected with an equivalent volume of PBS at the same locations. Following the injections, the animals were sutured and returned to normal housing conditions. At 1, 3, 7, and 10 months after  $\alpha$ -syn PFF injection, the mice were sacrificed. Truncal vagotomy is associated with a decreased risk for PD (Liu et al., 2017; Svensson et al., 2015). After the intestinal intramuscular  $\alpha$ -syn PFF injections, a full truncal vagotomy was performed in the same mouse (both male and female) (Figure S1A). The surgical procedure for vagotomy was as follows: (1) The vagus nerve was identified where it exits the diaphragm and the gastric branches were identified. From 2–3 mm above the cardia (the point where the esophagus and stomach connect to the diaphragm), a 4–6 mm section of each gastric branch was carefully isolated from the surrounding connective tissue and overlying vasculature (common carotid artery) and then excised. The neck incision was closed with black silk (5-0) (El-Salhy et al., 2000; Song et al., 2015). The abdominal incision was closed with sutures, and the skin incision was closed with wound clips. After mice underwent vagotomy, the mice were returned to the colony and the bedding and cage was evaluated up to twice daily to check their health. The surgical site was dressed with antibiotic ointment every day, until the wound healed (about 2 weeks). Soft gel feed was provided until the mice could perform normal activities. The body weight of the mice was measured 2 times per week. The vagotomy group was closely observed for weight loss, diet, and bowel movements. 7 months after vagotomy surgery, weight loss of approximately 18% was observed in the vagotomy group compared to the normal group.

### Behavioral tests

To evaluate  $\alpha$ -syn PFF-induced behavioral deficits, PBS and  $\alpha$ -syn PFF injected mice were assessed by the pole test, rotarod test, and grip strength test for motor deficits, and spontaneous alternation behavior Y-maze test, novel object recognition test, step-through passive avoidance test, Morris water maze test, nest building test, elevated plus maze, open field test, tail suspension

test, and forced swimming test for non-motor deficits 4-weeks prior to sacrifice. The experimenter was blinded to treatment group for all behavioral studies. All tests were performed and recorded between 10:00–16:00 in the lights-on cycle.

### Pole test

Mice were acclimatized in the behavioral procedure room for 30 min. The pole was composed of a 75 cm of metal rod with a diameter of 9 mm. It was wrapped with bandage gauze (Mao et al., 2016). Mice were placed on the top of the pole (7.5 cm from the top of the pole) facing the head-up. Total time taken to reach the base of the pole was recorded. Before the actual test, mice were trained for two consecutive days. Each training session consisted of three test trials. On the test day, mice were evaluated in three sessions and total time was recorded. The maximum cutoff time to stop the test and recording was 60 s. Results for turn down, climb down, and total time (in sec) were recorded.

### Rotarod test

For the rotarod test, the mice were trained 3 days before test. On day 4, mice were placed on an accelerating rotarod cylinder, and the latency time of the animals was measured. The speed was slowly increased from 4 to 40 rpm within 5 min. A trial ended if the animal fell off the rungs or gripped the device and spun around for 2 consecutive revolutions without attempting to walk on the rungs. Motor test data are presented as mean of latency time (3 trials) on the rotarod.

### Grip strength test

Neuromuscular strength testing was performed using a Bioseb grip strength test machine (BIO-GS3, Bioseb, FL USA) as previously described (Mao et al., 2016). Performance of the mice was assessed three times. To assess grip strength, mice were allowed to grasp a metal grid either by their fore limbs or both fore and hind limbs. The tail was gently pulled and the maximum holding force recorded by the force transducer when the mice released their grasp on the grid. The peak holding strength was digitally recorded and displayed as force in grams. Grip strength was scored as grams (g).

### Spontaneous alternation behavior Y-maze test

A spontaneous alternation behavior Y-maze test was performed as described (Kwon et al., 2009). The Y-maze is a horizontal maze with three equal angles between all arms, which were 40 cm long and 10 cm wide with 15 cm high walls. The maze floor and walls were constructed using opaque polyvinyl plastic. Mice were initially placed within one arm, and the sequence and number of arm entries were recorded manually for each mouse over an 8-min period. A spontaneous alternation was defined in which the mice entered all three arms, i.e., ABC, CAB, or BCA but not ABB, was recorded as an alternation to precision short-term memory. The alternation score (%) for each mouse was calculated as the ratio of the actual number of alternations to the possible number (defined as the total number of arm entries minus two) multiplied by 100 as shown by the following equation: % Alternative behavior =  $[(\text{Number of alternations})/(\text{Total arm entries} - 2)] \times 100$ . The number of arm entries per trial was used as an indicator of locomotor activity. The Y-maze arms were cleaned with diluted 10% ethanol between tests to eliminate odors and residues.

### Novel object recognition test (NORT)

The NORT was performed according to the method described previously (Bevins and Besheer, 2006). NORT were carried out in a gray open field box (45 cm width x 45cm depth x 50 cm height) with opaque polyvinyl plastic. Prior to the test, all mice were introduced to the test box for 5 min without objects. After the introduction period, animals were positioned into the open field box with two identical objects and allowed to explore for 5 min. The objects used in this experiment were wooden blocks with same size, but different shape. The time that mice spent on exploring each object was recorded (defined as the training session). Twenty-four hours after the training session, mice were allowed to search the objects for 5 min, in which the familiar object used in the training session was replaced with a novel object. The time spent by the mice exploring the novel and the familiar objects was recorded (defined as the test session). The animals were regarded to be exploring when they were sniffing, biting, or facing the object. The objects and test box were cleaned with 10% ethanol after each session. Data are expressed in percentage terms of novel object recognition time (time percentage =  $\text{total time spent with novel object} / [\text{total time spent with novel object} + \text{total time spent with familiar object}] \times 100$ ).

### Step-through passive avoidance test

The step-through passive avoidance apparatus is composed with one clear and one dark chamber, which are separated by a guillotine door. The floor of both the clear chamber (36 cm x 18 cm x 30 cm) and the dark chamber (36 cm x 18 cm x 30 cm) were composed of 2 mm stainless steel rods spaced 0.5 cm apart (Coulbourn Instruments, Holliston, MA, USA). The cue light positioned above clear chamber illuminated the apparatus. The mice underwent two separate trials: a training trial and a test trial 24 h later. For the acquisition trial, mice were initially placed in the clear chamber. When they entered the dark compartment, the door closed and an electrical foot shock (0.5 mA, 3 s duration) was delivered through the stainless steel rods. Twenty-four hours after the retention trial, mice were re-located in the illuminated compartment for the retention trial. The time taken for a mouse to enter the dark compartment after door opening was defined as latency for both training and test trials. Latency to enter the dark compartment was recorded up to 300 s.

### Morris water maze test (MWM)

The MWM was performed as described (Vorhees and Williams, 2006). The MWM is a white circular pool (150 cm in diameter and 50 cm in height) with four different inner cues on surface. The circular pool was filled with water and a nontoxic water-soluble white dye ( $20 \pm 1^\circ\text{C}$ ) and the platform was submerged 1 cm below the surface of water so that it was invisible at water level. The pool was divided into four quadrants of equal area. A black platform (9 cm in diameter and 15 cm in height) was centered in one of the four quadrants of the pool. The location of each swimming mouse, from the start position to the platform, was digitized by a video tracking system (ANY-Maze, Stoelting Co., Wood Dale, IL, USA). The day before the experiment mice were subjected to swim training for 60 s in the absence of the platform. The mice were then given two trial sessions each day for four consecutive days, with an inter-trial interval of 15 min, and the escape latencies were recorded. This parameter was averaged for each session of trials and for each mouse. Once the mouse located the platform, it was permitted to remain on it for 10 s. If the mouse was unable to locate the platform within 60 s, it was placed on the platform for 10 s and then returned to its cage by the experimenter. On day 6, the probe trial test involved removing the platform from the pool and mice were allowed the cut-off time of 60 s.

### Nest building test (NBT)

Nest building test was used to assess nigrostriatal sensorimotor and hippocampal cognitive functions in the mice (Fleming et al., 2004; Wu et al., 2016). This behavior requires the use of orofacial and forelimb movements, as the animals pull the nesting material apart with their forelimbs and teeth and subsequently break down the material in their mouths and incorporate it into their bedding. In brief, a 2.5 g nestlet (Johns Hopkins Medicine Research Animal Resources, Baltimore, MD, USA) was placed into the feeder of each cage. Pulling the cotton from the feeder requires the mice to rear up and to exercise complex fine motor skills. Nest-building scores were assessed, and the amount of unused nestlet material was measured after 16 h as an indicator of the nigrostriatal sensorimotor function of the mice (Deacon, 2006).

### Elevated plus maze (EPM)

The EMP test was performed according to the method described by Pellow (1986) with modifications (Pellow and File, 1986). The EPM consisted of two open arms (50 cm  $\times$  10 cm) and two closed arms with a wall (30 cm  $\times$  5 cm  $\times$  15 cm) connected to a central zone (5 cm  $\times$  5 cm), forming a cross. It was elevated to a height of 50 cm from the floor. A video camera was suspended above the maze to record the experiment. The maze floor and walls were constructed from opaque polyvinyl plastic and the open arms had a low (0.5 cm) edge. Each mouse was placed in the central intersection facing an open arm. The maze floor was cleaned thoroughly between trials using diluted 10% ethanol between tests to eliminate odors and residues. Both the time spent in the open arms and the number of entries into the open arms were recorded for a 5 min period using the Any-Maze behavioral tracking system. An entry was defined as all four paws in the arm. Both the time spent in the open arms and the number of entries into the open arms were converted into percentage of total time and entries, respectively.

### Open field test (OFT)

The open field consisted of a rectangular plastic box (40 cm  $\times$  40 cm  $\times$  40 cm) divided into 36 (6  $\times$  6) identical sectors (6.6 cm  $\times$  6.6 cm). The field was subdivided into peripheral and central sectors, where the central sector included 4 central squares (2  $\times$  2) and the peripheral sector was the remaining squares (Sakata et al., 2010). The mouse was placed into the center of an open field and allowed to explore for 5 min under dim light. The apparatus was thoroughly cleaned with diluted 10% ethanol between each trial. A video tracking system (ANY-Maze software) was used to record the distance traveled as a measure of locomotor activity. The time spent in and entries into the center were measured as an anxiolytic indicator (Sakata et al., 2010).

### Tail suspension test (TST)

The TST was carried out according to the method described by Steru et al. (Cryan et al., 2005; Steru et al., 1985). The mice were individually suspended in black Plexiglas boxes (50 cm  $\times$  50 cm  $\times$  50 cm) by the tail using an adhesive tape placed approximately 1 cm from the tip of the tail attached to a hook and hanging 5 cm above the floor. The immobility time was recorded using the video tracking system (ANY-Maze software) during a 6-min test.

### Forced swimming test (FST)

The FST was carried out on mice according to the method of Porsolt (Porsolt et al., 1978). Briefly, mice were individually introduced to a glass cylinder (20 cm in height, 14 cm in diameter) filled 16 cm high with water ( $25 \pm 1^\circ\text{C}$ ). After a 6-min forced swim test session, the immobility time during the final 4-min interval of the test was determined and analyzed using the video tracking system (ANY-Maze software). Immobility time was considered to be a mouse floating passively, making only small movements to keep its nose above the surface.

### Buried pellet test (BPT)

The buried pellet test (BPT) was performed as previously described (Fleming et al., 2008; Talaga et al., 2017). Individually housed mice were food restricted and maintained at  $\sim 90\%$  body weight for 2 days prior to and during testing. Food-restricted mice were given 0.2 g of mouse chow per animal per day depending on weight. Weights were monitored each day during food restriction.

The BPT was performed for 4 days and the surface pellet control test was performed for one trial one day after the buried pellets. For the buried pellet trial test, a clean mouse cage (15 cm  $\times$  25 cm  $\times$  13 cm) was filled with clean bedding 3 cm deep. Two pieces of sweetened cereal (Cinnamon Toast Crunch; General Mills Inc., Federalburg, MD, USA) was buried along the perimeter of the cage approximately 0.5 cm below the bedding so that it was not visible. The latency to find the first pellet was recorded when the mouse touched the pellet. After the mouse located the first pellet, it was allowed to consume it. Failure to find the food pellet within 5 min resulted in the pellet being removed, the trial mouse was returned to its cage and given a score of 5 min. The bedding was changed between mice for all testing periods and the cereal was buried in a different location on each test day. The visible pellet trial test was set up in a similar way except that the piece of cereal was placed on top of the bedding.

### Single Photon Emission Computed Tomography-Computed Tomography (SPECT/CT) imaging in mice

Mice were introduced to and housed in the scanner room 24 h prior to scanning for acclimation. Each mouse was injected intravenously with 17 MBq (SA > 20,000 Ci/mmol, 500  $\mu$ Ci) of [ $^{123}$ I]ioflupane (Cardinal Health, Dublin, OH) and then observed for a 4 h uptake period inside the home cage. Mice were scanned sequentially in pairs under 2% isoflurane in oxygen using a Molecular Imaging VECTOR SPECT imager equipped with a mouse 0.6 mm multipinhole collimator. 30 min acquisitions over the skull were performed in listmode where 160 keV events were collected. Data were reconstructed using the manufacturer's software using ML-EM with up to 30 iterations at 0.2 mm resolution. Anatomic CT scans were performed on a Sedecal SuperArgus PET/CT scanner (Madrid Spain) at 65 kVp, 720 slices and 100  $\mu$ m resolution. CT images were reconstructed using the manufacturer's software. All data were visualized, co-registered and quantitated using AMIDE (<http://amide.sourceforge.net/>). Quantitation involved drawing ROIs over each (left versus right) caudate-putamen based on total SPECT signal in each slice and comparing uptake (nCi/cc) within each mouse and between mice.

### Immunohistochemistry and quantitative analysis

Mice were perfused with ice-cold PBS followed by fixation with 4% paraformaldehyde/PBS (pH 7.4). Brains were collected and post-fixed for 16 h in 4% paraformaldehyde and cryoprotected in 30% sucrose/PBS (pH 7.4) solution. Brains were frozen in OCT buffer and 30  $\mu$ m serial coronal sections were cut with a microtome. Free-floating 30  $\mu$ m sections were blocked with 4% goat or horse serum/PBS plus 0.2% Triton X-100 and incubated with an antibody against TH (Novus Biologicals, Littleton, CO, USA), an antibody against ChAT (Abcam, Billerica, MA, USA), and an antibody against pSer129- $\alpha$ -syn (Biolegend, San Diego, CA, USA) followed by incubation with biotin-conjugated anti-rabbit antibody or biotin-conjugated anti-mouse antibody (Vectastain Elite ABC Kit, Vector laboratories, Burlingame, CA, USA). After developing using SigmaFast DAB Peroxidase Substrate (Sigma-Aldrich), sections were counterstained with Nissl (0.09% thionin). TH-positive and Nissl positive DA neurons from the SNc region, and ChAT-positive cholinergic neurons from the DMV region were counted through optical fractionators, the unbiased method for cell counting by using a computer-assisted image analysis system consisting of an Axiophot photomicroscope (Carl Zeiss Vision) equipped with a computer controlled motorized stage (Ludl Electronics), a Hitachi HV C20 camera, and Stereo Investigator software (MicroBright-Field). Fiber density in the striatum was analyzed by optical density (OD) measurement using ImageJ software (NIH, <https://imagej.nih.gov/ij/>). The number of pSer129- $\alpha$ -syn positive and Nissl positive staining from the duodenum to the olfactory bulb region were measured with ImageJ software. Four areas of interest (1024 pixel  $\times$  1024 pixel) within each tissue section were analyzed to estimate the average number of pSer129- $\alpha$ -syn positive neurons by field counting, and the data are presented as pSer129- $\alpha$ -syn positive cells per mm<sup>2</sup>.

### Immunofluorescence analysis

Immunofluorescence was performed on 30  $\mu$ m thick serial brain sections as described previously with some modifications (Mao et al., 2016). Briefly, 4% Paraformaldehyde/PBS (pH 7.4)-fixed coronal brain sections were blocked with 10% donkey serum (Jackson ImmunoResearch)/PBS plus 0.3% Triton X-100 and incubated with antibodies to pSer129- $\alpha$ -syn (Biolegend), TH (Novus Biologicals), and Tuj1 (Biolegend) or antibodies to pSer129- $\alpha$ -syn (Biolegend) and Cy3 conjugated NeuN (Millipore, Temecula, CA, USA) overnight at 4°C. After washes with PBS, floating brain sections were incubated with 0.1% Triton X-100 and 5% donkey serum in PBS, followed by 1 h of incubation with a mixture of FITC-conjugated (Jackson ImmunoResearch) and CY3-conjugated (Jackson ImmunoResearch) secondary antibodies at RT. The fluorescent images were acquired via a Zeiss confocal microscope (Zeiss Confocal LSM 710) after the coverslips were mounted with DAPI mounting solution (VECTASHIELD HardSet Antifade Mounting Medium with DAPI, Vector laboratories). All images were processed by the Zeiss Zen software. The selected area in the signal intensity range of the threshold was measured using ImageJ analysis.

### Tissue lysate preparation

Tissue lysates were prepared as described previously with some modifications (Mao et al., 2016). Nonionic detergent-soluble and -insoluble fractions were prepared by sequential lysis buffer. Tissues were homogenized in the following lysis buffer [10 mM Tris-HCl, pH 7.4, 150 mM NaCl, 5 mM EDTA, 1% Triton X-100, phosphatase inhibitor cocktail II and III (Sigma-Aldrich), and complete protease inhibitor mixture (Sigma-Aldrich)], and then were centrifuged and soluble supernatant was collected. The insoluble pellet was washed once in brain lysis buffer containing nonionic detergent (0.1% Triton X-100) and the resulting pellet was lysed with lysis buffer containing 2% SDS and 0.5% sodium deoxycholate. The homogenate was centrifuged and the resulting supernatant (Triton X-100 detergent-insoluble) was collected. Total lysates were prepared by homogenization of tissue in RIPA buffer [50 mM Tris,

pH 8.0, 150 mM NaCl, 1% Nonidet P-40, 1% SDS, 0.5% sodium-deoxycholate, phosphatase inhibitor cocktail II and III (Sigma-Aldrich), and complete protease inhibitor mixture (Sigma-Aldrich)]. After homogenization, samples were rotated at 4°C for 30 min for complete lysis, the homogenate was centrifuged at 22,000  $\times$  g for 20 min and the supernatants were collected. Protein levels were quantified using the BCA Kit (Pierce, Rockford, IL, USA) with BSA standards and analyzed by immunoblot.

### Immunoblot analysis

Electrophoresis on 8%–16% and 4%–20% gradient SDS-PAGE gels was performed on 10–20  $\mu$ g of proteins from the mouse brain tissue. The proteins were then transferred to nitrocellulose membranes. The membranes were blocked with blocking solution (Tris-buffered saline with 5% non-fat dry milk and 0.1% Tween-20) for 1 h and incubated at 4°C overnight with anti-TH (Novus Biologicals), anti-DAT (Sigma-Aldrich), anti- $\alpha$ -synuclein (BD Biosciences, San Jose, CA, USA), anti-pSer129- $\alpha$ -syn (Abcam) antibodies, followed by HRP-conjugated rabbit of mouse secondary antibodies (1:50,000, GE Healthcare, Pittsburgh, PA, USA) for 1 h at RT. Primary antibodies and working dilutions are detailed in the [Key Resources Table](#). The bands were visualized by enhanced chemiluminescence (Thermo Scientific, IL, USA). Finally, the membranes were re-probed with HRP-conjugated  $\beta$ -actin antibody (1:40,000, Sigma-Aldrich) after it was stripped.

### Assessments of body weight change, food intake, serum ghrelin levels, and fecal output

One month before the experiments, baseline body weight and food intake were measured by housing the mice in individual cages. 20 g of food pellets were provided to the individual cages for measurement of food consumption at 6 and 12 h. Body weight was recorded before injection with PFF and one month after the PFF injection. For the assessment of fecal output, individually housed mice were removed from their home cages and placed in a 20 cm  $\times$  20 cm opaque disposable cylinder at the end of a 12 h light and dark cycle. Fecal pellets were counted every 5 min, over 30 min. Serum ghrelin levels after 48 h of fasting were measured using a mouse ghrelin EIA kit (Phoenix Pharmaceuticals, Belmont, CA, USA). Blood sampling was performed by cardiac puncture. Blood was quickly transferred to EDTA-treated tubes and spun for serological analysis. PBS or PFF injected WT and TV mice sera were incubated in a secondary antibody pre-coated immunoplate for 2 h at RT. After four washes with assay buffer, streptavidin-HRP solution was added and incubated for 1 h at RT. After four washes, the immunoplate was incubated with 3,3',5,5'-tetramethylbenzidine (TMB) for 1 h at RT. 2N HCl was added to the immunoplate to terminate reaction, and OD at 450 nm was determined by a microplate reader.

### Monoamine analysis

High performance liquid chromatography with electrochemical detection (HPLC-ECD) was performed to measure biogenic amine concentrations as described previously ([Karuppagounder et al., 2014](#)). Briefly, striatal tissues were weighed and sonicated in 0.2 mL of ice cold 0.01 mM perchloric acid containing 0.01% EDTA and 60 ng of 3,4-dihydroxybenzylamine (DHBA) as an internal standard followed by centrifugation (15,000  $\times$  g, 30 min, 4°C). The supernatant was passed through a 0.2 mm filter and 20  $\mu$ L of the filtered supernatant was injected to the HPLC column (3.0 mm  $\times$  150 mm C-18 reverse phase column, Atlantis T3 3  $\mu$ m) using a dual channel coulchem III electrochemical detector (Model 5300, ESA Inc., Chelmsford, MA, USA). Protein concentrations of tissue homogenates were measured using BCA protein assay kit (Pierce, Rockford, IL, USA). Data were normalized to protein concentration and expressed in ng/ $\mu$ g protein.

## QUANTIFICATION AND STATISTICAL ANALYSIS

All data were analyzed using GraphPad Prism 6 software. Statistics Data are presented as the mean  $\pm$  SEM with at least 3 independent experiments. Representative morphological images were obtained from at least 3 experiments with similar results. Statistical significance was assessed via a one or two-way ANOVA test followed by Bonferroni post hoc multiple comparison analysis. Assessments with  $p < 0.05$  were considered significant.

## DATA AND CODE AVAILABILITY

All raw data for this study is deposited on Mendeley and can be found at <https://doi.org/10.17632/swzrgbp3p5.1>.